

Analysis of the low-energy π^-p charge-exchange data

E. Matsinos*^a, G. Rasche^b,

^a*Centre for Applied Mathematics and Physics, Zurich University of Applied Sciences, Technikumstrasse 9, P.O. Box, CH-8401 Winterthur, Switzerland*

^b*Institut für Theoretische Physik der Universität, Winterthurerstrasse 190, CH-8057 Zürich, Switzerland*

*Corresponding author. E-mail: evangelos.matsinos@zhaw.ch, evangelos.matsinos@sunrise.ch; Tel.: +41 58 9347882; Fax: +41 58 9357306

Abstract

We analyse the charge-exchange (CX) measurements $\pi^-p \rightarrow \pi^0n$ below pion laboratory kinetic energy of 100 MeV. After the removal of five degrees of freedom from the initial database, we combine it with the truncated π^+p database of Ref. [1] and fit the ETH model [6] to the resulting data. The set of the parameter values of the ETH model, as well as the predictions derived on their basis for the hadronic phase shifts and for the low-energy πN constants, are significantly different from the results obtained in the analysis of the truncated $\pi^\pm p$ elastic-scattering databases. The main difference in the hadronic phase shifts occurs in $\tilde{\delta}_{0+}^{1/2}$. We discuss the implications of these findings in terms of the violation of the isospin invariance in the hadronic part of the πN interaction. The effect observed amounts to the level of 7 – 8% in the CX scattering amplitude below 70 MeV. The results and conclusions of this study agree well with those obtained in the mid 1990s, when the isospin invariance was first tested by using πN experimental data, and disagree with the predictions obtained within the framework of the heavy-baryon Chiral-Perturbation Theory.

PACS: 13.75.Gx; 25.80.Dj; 25.80.Gn

Key words: πN hadronic phase shifts; πN coupling constants; πN threshold parameters; isospin-invariance violation; isospin breaking

1 Introduction

This is the last of three papers addressing issues of the pion-nucleon (πN) interaction at low energies (pion laboratory kinetic energy $T \leq 100$ MeV). In the first paper [1], we reported on a new phase-shift analysis (PSA) of the $\pi^\pm p$ elastic-scattering measurements. In the second paper [2], we examined the self-consistency of the $\pi^\pm p$ elastic-scattering differential cross sections of Ref. [3], which we have not included in our PSAs. In the present study, we will analyse the experimental data for the charge-exchange (CX) reaction $\pi^- p \rightarrow \pi^0 n$ and investigate whether earlier claims on the isospin breaking [4,5] need to be revised in view of the impressive increase of the CX database and of the development of our analysis methods during the last fifteen years.

We will mark the physical quantities extracted in the PSA of the $\pi^\pm p$ elastic-scattering data [1] with the label ‘ZUAS12’; this applies both to the solution obtained for the parameters of the ETH model [6], as well as to the predictions derived on the basis of Tables 3 (for $p_{min} \approx 1.24 \cdot 10^{-2}$, where p_{min} denotes the confidence level for the acceptance of the null hypothesis, i.e., of no statistically-significant effects) and 4 of Ref. [1]. The corresponding results, obtained in the present work from the common analysis of the $\pi^\pm p$ and CX databases, will be marked with the label ‘ZUAS12a’.

Similarly to Ref. [1], we will assume that the physical quantities appearing in the present study (i.e., the fit parameters of Sections 5.1 and 5.2, the scattering lengths and volumes of Section 5.2.1, the hadronic phase shifts of Section 5.2.2, etc.) are not purely-hadronic quantities since they still contain residual electromagnetic (em) effects. The repetitive use of the term ‘em-modified’ is clumsy; therefore, we will omit it, unless we consider its use necessary as, for instance, in the captions of the tables and figures, as well as in Section 8.

2 Method

The formalism which we use here has been described in detail in Ref. [7]. The determination of the observables from the hadronic phase shifts may be found in Section 2 of that work. For $\pi^\pm p$ scattering, one obtains the partial-wave amplitudes from Eq. (1) and determines the no-spin-flip and spin-flip amplitudes via Eqs. (2) and (3). The observables are obtained from these amplitudes via Eqs. (13) and (14). For the CX reaction, the observables are determined using Eqs. (21-24) of Ref. [7].

All the details on the analysis method (i.e., on the minimisation function, on the scale factors, etc.) may be found in Section 2.2 of Ref. [1]. The contribution

χ_j^2 of the j^{th} data set to the overall χ^2 is given therein by Eq. (1). The scale factors z_j , which minimise each χ_j^2 , are evaluated using Eq. (2); the minimal χ_j^2 value for each data set (denoted by $(\chi_j^2)_{\text{min}}$) is given in Eq. (3) and the scaling contribution (of the j^{th} data set) to $(\chi_j^2)_{\text{min}}$ in Eq. (4). Finally, the scale factors for free floating \hat{z}_j (which we will use in Section 6, when investigating the absolute normalisation of the CX data using the ZUAS12 prediction as reference) are obtained from Eq. (5); their total uncertainty $\Delta\hat{z}_j$ has been defined at the end of Section 2.2 of Ref. [1].

One statistical test will be performed on each data set, involving its contribution $(\chi_j^2)_{\text{min}}$ to the overall χ^2 . The corresponding p-value will be evaluated from the $(\chi_j^2)_{\text{min}}$ and the number of degrees of freedom of the data set (hereafter, the acronym DOF will stand for ‘degree(s) of freedom’, whereas NDF will denote the ‘number of DOF’); for a data set with N_j data points (none of which is an outlier), NDF is equal to N_j . Decisions on the tested data set will be made on the basis of the comparison of the corresponding p-value with the assumed confidence level p_{min} . The value of p_{min} is fixed to the equivalent of a 2.5σ effect in the normal distribution, corresponding to about $1.24 \cdot 10^{-2}$.

The repetitive referencing to the databases is largely facilitated if one adheres to the following notation: DB_+ for the π^+p database; DB_- for the π^-p elastic-scattering database; DB_0 for the CX database; $\text{DB}_{+/-}$ for the combined $\pi^\pm p$ elastic-scattering databases; $\text{DB}_{+/0}$ for the combined π^+p and CX databases. Furthermore, the prefix ‘t’ (as, for instance, in tDB_+) denotes a ‘truncated’ database, i.e., a database obtained after the removal of the outliers.

3 The CX data

The available measurements are listed (in the chronological order they had been reported) in Table 1. During the last fifteen years, the database has been enlarged by a factor of seven, i.e., from a mere 47 data points (which were available for the analyses [4,5]) to the present status of a total of 333 data points. Of the added 286 data points, 270 relate to the differential cross section (DCS), 9 to the total cross section (TCS), 6 to the analysing power (AP), and 1 data point to one threshold constant (to the isovector scattering length b_1).

A milestone in the low-energy CX experimentation was the FITZGERALD86 [11] experiment, which took place at LAMPF and used the π^0 spectrometer to obtain (for the first time) important DCS data around the s - and p -wave interference minimum (see next section). By establishing a rigorous relation between the real parts of the s - and p -wave CX amplitudes at low energies, the FITZGERALD86 experiment became the backbone of the analyses [4,5]

and was essential in terms of their conclusions on the violation of the isospin invariance in the hadronic part of the πN interaction. The FITZGERALD86 experiment was the first complete CX experiment, as it also investigated (and reported) the normalisation uncertainty. Important in terms of the enhancement of the DB_0 was the ISENHOWER99 [16] experiment, also performed at LAMPF with the π^0 spectrometer.

Within the last decade, the Crystal-Ball Collaboration made massive contributions to the low-energy DB_0 with experiments at the Brookhaven National Laboratory (BNL): the SADLER04 [18] experiment added 60 data points, whereas the successor of that experiment, the MEKTEROVIĆ09 [21] experiment, contributed another 140 data points. In total, the data obtained by the Crystal-Ball Collaboration amount now to 60% of the DB_0 which is available below 100 MeV.

From the remaining experiments, the JIA08 [20] data have been taken around the s - and p -wave interference minimum, whereas the SCHROEDER01 [17] experimental result on the width of the $1s$ state of pionic hydrogen (corrected in Ref. [22] after properly taking into account the contributions of the γn channel) led to the extraction of the scattering length \tilde{a}^{c0} ($= \sqrt{2}b_1$). The FRLEŽ98 [14] experiment investigated the angular distribution of the DCS at 27.50 MeV. Finally, the BREITSCHOPF06 [19] experiment reported the TCSs at nine energies below 100 MeV. The remaining experiments account for less than 10% of the DB_0 at low energies.

The complete DB_0 consists of 54 data sets. The quoted values of the TCS in Refs. [10,12,21] have been extracted from the coefficients of the Legendre expansion of the angular distribution of the DCS and are thus correlated with the main results of these experiments; because of this correlation, one may use either set of values, but not both. We will use the Legendre coefficients of Refs. [10,12] (their DCS measurements have not been published), and directly the DCS data of Ref. [21].

In our approach, all data sets must be accompanied by a normalisation uncertainty. This requirement also applies to one-point data sets, because the scale factors must be calculated in all cases (in order to enable the investigation of a possible bias in the analysis). As a result, realistic normalisation uncertainties had to be assigned to those experiments which did not report this quantity. We decided to assign these uncertainties as follows:

- 6% to BUGG71 [8], as this uncertainty was assigned to the experiments of the TCS or PTCS in Refs. [1,7].
- 3% to BREITSCHOPF06, because the experimental group had already combined statistical and systematic effects in quadrature (and reported only the total uncertainty).

- 3.1% to SALOMON84 [10], i.e., the normalisation uncertainty of the (similar, as well as close in time) BAGHERI88 [12] experiment.
- 8% to DUCLOS73 [9], i.e., double the normalisation uncertainty of the ISENHOWER99 large-angle data sets.

The experimental results of Ref. [20] contain asymmetric statistical uncertainties for the measured DCS. Unable to treat asymmetric uncertainties in the analysis, we will use the average of the (absolute values of the) two uncertainties for each input data point.

4 The s - and p -wave interference minimum

The main contributions to the CX scattering amplitude in the low-energy region come from the real parts of the s and p waves. These contributions are of opposite signs and cancel each other in the forward direction around 45 MeV. This destructive-interference phenomenon acts as a magnifying glass, probing the smaller contributions in the πN dynamics, like those from the imaginary parts, from the d and f waves, and (potentially) from isospin breaking.

An estimate of the energy of the CX DCS minimum had been obtained in the FITZGERALD86 experiment, from a fit to the extrapolated DCS values to centre-of-mass (CM) scattering angle $\theta = 0^\circ$. According to that estimate, the CX DCS minimum occurs at $T = 45.0 \pm 0.5$ MeV; the minimal DCS value was also extracted: $\left(\frac{d\sigma}{d\Omega}\right)_{min} = 2.4 \pm 0.5 \mu\text{b/sr}$ [11]. The ZUAS12 predictions¹ are 43.7 ± 0.1 MeV and $0.3 \pm 0.1 \mu\text{b/sr}$, respectively.

5 Results of the fits to the CX measurements

5.1 Fits to the DB_0 using the K -matrix parameterisations

For $T \leq 100$ MeV, each K -matrix element (i.e., each phase shift) can be approximated in terms of a finite number of energy-independent expansion parameters. The explicit forms of the parameterisations, used in the present work, have been given in Ref. [1]. Since the presently-available experimental

¹ The statistical uncertainty in the prediction for the energy T of the CX DCS minimum was well below the quoted value. We opt for an increased uncertainty as we have not investigated the sensitivity of the extracted result to the variation of the d and f waves, which we have fixed herein (as in Ref. [1]) from the current SAID solution (WI08) [23].

data in the energy domain of our analyses cannot determine the expansion coefficients of higher-order terms, we retain in our parametric forms only the terms up to $\mathcal{O}(\epsilon^2)$, where ϵ is the pion CM kinetic energy ². As when analysing the DB₋ in Section 3.2 of Ref. [1], we will fix the $I = 3/2$ amplitudes from the final fit to the tDB₊ using the K -matrix parameterisations (see Section 3.1 of that paper). The same K -matrix parameterisations for the $I = 1/2$ amplitudes will be used in the description of the CX measurements, with different parameters $\tilde{a}_{0+}^{1/2}$, b_1 , c_1 , d_{13} , e_{13} , d_{11} , and e_{11} . (The fit parameter b_1 is not the standard isovector scattering length defined in Section 3.)

The results of the optimisation procedure are shown in Table 2. Since seven parameters are used to generate the fitted values, the NDF in the first fit to the DB₀ was 326; the minimum value of χ^2 was 400.3, indicating a rather coherent database. For the tDB₀, the minimum value of χ^2 was 312.8 for 321 DOF in the fit. The optimal values of the parameters $\tilde{a}_{0+}^{1/2}$, d_{13} , and e_{13} came out significantly different ³ from those obtained in the analysis of the tDB₋ in Ref. [1]. The details on the tDB₀, obtained from the final fit, are given in Table 3.

Although the results of Tables 2 and 3 provide ground for questioning the absolute normalisation of all seven FITZGERALD86 data sets, we decided to retain the absolute normalisation of the three remaining FITZGERALD86 data sets as their removal is not called for when strictly applying our rejection criteria. On the other hand, given the importance of FITZGERALD86 data in the analyses of Refs. [4,5], it goes without saying that the re-analysis of the CX measurements in terms of the violation of the isospin invariance in the hadronic part of the πN interaction at low energies is imperative.

5.2 Common fit to the tDB_{+/0} using the ETH model

Details on the ETH model, as well as on its seven parameters (G_σ , K_σ , G_ρ , K_ρ , $g_{\pi NN}$, $g_{\pi N\Delta}$, and Z), may be obtained from Refs. [1,7]. This isospin-invariant model was introduced in Ref. [6] and was developed to its final form by the

² As in any phenomenological description of data, there is some arbitrariness in the choice of the forms used in our K -matrix parameterisations (e.g., using ϵ or the square of the CM momentum as expansion variable, expanding K or K^{-1} , etc.). The chosen forms achieve the best reproduction of the experimental data, allowing simultaneously the determination of the fit parameters from the available πN data below 100 MeV. In general, the differences among the solutions, obtained with the forms which were examined, were found small (e.g., the differences in the resulting χ^2 values were typically at the percent level).

³ The differences between the two sets of values represent effects between 4.9 and 7.4σ in the normal distribution.

mid 1990s.

Prior to fitting the ETH model to the $\text{tDB}_{+/0}$, the data were subjected to a common fit using the K -matrix parameterisations. The tDB_+ consisted of 340 data points (detailed in Table 1 of Ref. [1]), whereas the tDB_0 comprised 328 data points, i.e., the original 333 data points minus the five outliers detailed in Table 2 of this work. The common fit to these data using the K -matrix parameterisations resulted in the χ^2 value of 737.0 for 654 DOF and no additional outliers.

The model fit to the data yielded the minimal χ^2 value of 960.5 for 661 DOF. The optimal values of the model parameters from the fit to the $\text{tDB}_{+/0}$ are listed in Table 4; the uncertainties contain the Birge factor $\sqrt{\chi^2/\text{NDF}}$, which takes account of the goodness of the fit. The table also contains the ZUAS12 solution for $p_{\min} \approx 1.24 \cdot 10^{-2}$. The differences between these two sets of values are evident, especially for G_ρ and $g_{\pi NN}$. The correlation (Hessian) matrix, obtained in the fit, is given in Table 5.

We now reflect on the final χ^2 values obtained so far. We first concentrate on the results for $p_{\min} \approx 1.24 \cdot 10^{-2}$. The separate fits to the data using the K -matrix parameterisations yielded the χ^2 values of 427.2, 371.0 [1], and 312.8 (this work) for the tDB_+ , tDB_- , and tDB_0 , with 333, 321, and 321 DOF, respectively. The χ^2 values obtained with the K -matrix parameterisations in the two analyses of the combined truncated databases (i.e., $\text{tDB}_{+/-}$ and $\text{tDB}_{+/0}$) come out very close to the sum of the corresponding results for the separate fits: 792.4 (instead of the sum of 798.1) for the $\text{tDB}_{+/-}$ [1] and 737.0 (instead of the sum of 740.0) for the $\text{tDB}_{+/0}$ (this work). (As the NDF in the tDB_- and tDB_0 are (by chance) identical, the results are directly comparable.) Therefore, we observe that, in the case of the fits using the K -matrix parameterisations, the difference of the two χ^2 values (which is about 55.4) reflects, almost entirely, the difference of the χ^2 values in the separate fits to the tDB_- and tDB_0 (which is equal to 58.1, the smaller χ^2 value for the fit to the tDB_0).

The increase of the χ^2 values in the fits to the $\text{tDB}_{+/-}$ or to the $\text{tDB}_{+/0}$ using the ETH model (over the result of the fits to the same data using the K -matrix parameterisations) is due to the imposition of theoretical constraints (e.g., of the crossing and isospin symmetry); as earlier mentioned, the fits to the data using the K -matrix parameterisations are devoid of theoretical constraints, other than the expected low-energy behaviour of the K -matrix elements. All else being equal, one would expect that the difference in the χ^2 values between the model fit to the data and the fit using the K -matrix parameterisations would (more or less) be the same for the two truncated databases, i.e., for the $\text{tDB}_{+/-}$ and $\text{tDB}_{+/0}$; however, this is far from being true. The value of +55.4 for the difference $\chi^2(\text{tDB}_{+/-}) - \chi^2(\text{tDB}_{+/0})$ in the

fits using the K -matrix parameterisations turns into -87.6 with the use of the ETH model. This is the result of the considerably larger increase in the χ^2 for the $\text{tDB}_{+/0}$ fits from the K -matrix parameterisations to the use of the ETH model: this increase amounts to 223.5 compared to 80.5 for the $\text{tDB}_{+/-}$ fits ⁴. Evidently, the substitution of the tDB_- with tDB_0 leads to a noticeable deterioration of the overall description of the experimental data in the model fits. This deterioration is a first indication of a general difficulty in the description of the $\text{tDB}_{+/0}$ in terms of *one* set of parameter values of the ETH model. This fact can be explained if the theoretical basis upon which the data analysis rests (presumably, the isospin invariance in the hadronic part of the πN interaction) is somewhat disturbed. Inspection of Table 6 reveals that the information which is obtained from the results for the two other p_{min} levels used in Ref. [1] (i.e., those corresponding to a 2 and 3 σ effect in the normal distribution) matches very well the result for $p_{min} \approx 1.24 \cdot 10^{-2}$. We will return to this issue in Section 7.3.

5.2.1 Threshold constants

From the values of the model parameters and their uncertainties given in Table 4, as well as the correlation matrix given in Table 5, we calculated the isoscalar and isovector s -wave scattering lengths and the isoscalar(isovector)-scalar(vector) p -wave scattering volumes. The results are:

$$\begin{aligned}
\frac{1}{3} \tilde{a}_{0+}^{1/2} + \frac{2}{3} \tilde{a}_{0+}^{3/2} &= 0.0059(25) \mu_c^{-1}, \\
-\frac{1}{3} \tilde{a}_{0+}^{1/2} + \frac{1}{3} \tilde{a}_{0+}^{3/2} &= -0.08245(56) \mu_c^{-1}, \\
\frac{1}{3} \tilde{a}_{1-}^{1/2} + \frac{2}{3} \tilde{a}_{1-}^{3/2} + \frac{2}{3} \tilde{a}_{1+}^{1/2} + \frac{4}{3} \tilde{a}_{1+}^{3/2} &= 0.2103(30) \mu_c^{-3}, \\
-\frac{1}{3} \tilde{a}_{1-}^{1/2} + \frac{1}{3} \tilde{a}_{1-}^{3/2} - \frac{2}{3} \tilde{a}_{1+}^{1/2} + \frac{2}{3} \tilde{a}_{1+}^{3/2} &= 0.1829(17) \mu_c^{-3}, \\
\frac{1}{3} \tilde{a}_{1-}^{1/2} + \frac{2}{3} \tilde{a}_{1-}^{3/2} - \frac{1}{3} \tilde{a}_{1+}^{1/2} - \frac{2}{3} \tilde{a}_{1+}^{3/2} &= -0.1940(18) \mu_c^{-3}, \\
-\frac{1}{3} \tilde{a}_{1-}^{1/2} + \frac{1}{3} \tilde{a}_{1-}^{3/2} + \frac{1}{3} \tilde{a}_{1+}^{1/2} - \frac{1}{3} \tilde{a}_{1+}^{3/2} &= -0.0697(11) \mu_c^{-3}.
\end{aligned} \tag{1}$$

Converting these results to the standard spin-isospin quantities, we obtain

$$\tilde{a}_{0+}^{3/2} = -0.0765(25) \mu_c^{-1}, \quad \tilde{a}_{0+}^{1/2} = 0.1708(29) \mu_c^{-1},$$

⁴ The importance of these differences may be easily assessed after considering that the variance of the χ^2 distribution is equal to $2 \cdot \text{NDF}$; therefore, the expectation for the ‘statistical fluctuation’ in the quoted χ^2 values is $\sqrt{2 \cdot \text{NDF}}$.

$$\begin{aligned}\tilde{a}_{1+}^{3/2} &= 0.2190(19) \mu_c^{-3}, & \tilde{a}_{1+}^{1/2} &= -0.0337(12) \mu_c^{-3}, \\ \tilde{a}_{1-}^{3/2} &= -0.0447(13) \mu_c^{-3}, & \tilde{a}_{1-}^{1/2} &= -0.0883(22) \mu_c^{-3}.\end{aligned}\tag{2}$$

Significant differences are found when comparing the values of $\tilde{a}_{0+}^{1/2}$, $\tilde{a}_{1+}^{3/2}$, and $\tilde{a}_{1-}^{1/2}$ with the corresponding results of Ref. [1].

From the results in Eqs. (2), we obtain

$$\tilde{a}^{cc} = \frac{2}{3} \tilde{a}_{0+}^{1/2} + \frac{1}{3} \tilde{a}_{0+}^{3/2} = 0.0884(26) \mu_c^{-1}$$

and

$$\tilde{a}^{c0} = \sqrt{2} \left(-\frac{1}{3} \tilde{a}_{0+}^{1/2} + \frac{1}{3} \tilde{a}_{0+}^{3/2} \right) = -0.11660(79) \mu_c^{-1}.$$

Unlike the \tilde{a}^{cc} value extracted from the tDB_{+/-} [1], the value of the present work is compatible with the result of the measurement of the strong shift of the 1s state of pionic hydrogen [17]. Additionally, the value of \tilde{a}^{c0} is marginally consistent (the difference between the two values is at the level of 1.9σ) with the result of the same experiment for the width of the 1s state of pionic hydrogen. (In this comparison, the em corrections of Ref. [22] have been applied to the raw experimental results of Ref. [17].)

5.2.2 Hadronic phase shifts

The results for the *s*- and *p*-wave phase shifts, from the fit to the tDB_{+/0} using the ETH model, are given in Table 7. These hadronic phase shifts are also shown in Figs. 1-6, together with the ZUAS12 results, as well as the current SAID solution (WI08) [23] and their five single-energy values (wherever available). A very noticeable difference is seen in the case of $\tilde{\delta}_{0+}^{1/2}$. Smaller differences may be seen in two *p*-wave phase shifts, i.e., in $\tilde{\delta}_{1+}^{3/2}$ and $\tilde{\delta}_{1-}^{1/2}$.

5.2.3 Scale factors and normalised residuals

Similarly to the tests performed in Section 3.4.4 of Ref. [1], we will first investigate whether any bias is present in the distribution of the scale factors z_j , extracted in the final step of the optimisation scheme. Subsequently, we will address the issue of the distribution of the normalised residuals of the fit.

Two linear fits (the pion laboratory kinetic energy being the independent variable) to the optimal z_j values of Figs. 7 (for the π^+p) and 8 (for the CX

reaction) were performed. The results of these two fits do not match well. The two intercept values were: 0.972 ± 0.019 in the case of the π^+p reaction and 1.062 ± 0.016 for the CX reaction. The slope was found to be compatible with 0 in the former case: $(2.6 \pm 2.5) \cdot 10^{-4} \text{ MeV}^{-1}$. A noticeable energy dependence was found in the latter; the slope value came out equal to $(-6.8 \pm 2.7) \cdot 10^{-4} \text{ MeV}^{-1}$.

In Section 5.1, we questioned the determination of the absolute normalisation in the FITZGERALD86 experiment, yet allowed three of these data sets to take part in the optimisation (as our criteria for rejection were not fulfilled). The fitted values of the intercept and slope are almost left intact in case the scale factors of these three data sets are not included in the linear fit examining the energy dependence of the scale factors; the intercept value came out equal to 1.060 ± 0.014 , whereas the slope $(-6.9 \pm 2.4) \cdot 10^{-4} \text{ MeV}^{-1}$. It may also be argued that the extracted values of the intercept and of the slope show sensitivity to the inclusion in the fit of the three low-energy (10.60 MeV) entries of the ISENHOWER99 experiment (which we have no reason to question). We removed these three entries from the input and repeated the fit (also continuing to exclude the three afore-mentioned FITZGERALD86 entries); the intercept value came out equal to 1.053 ± 0.016 , whereas the slope $(-5.9 \pm 2.7) \cdot 10^{-4} \text{ MeV}^{-1}$.

These results establish a rather problematic situation (from the point of view of the analysis of the measurements with the ETH model) when forcing the data of these two reactions into a common optimisation scheme; the different values of the two intercepts demonstrate the overall tendency in the optimisation, with the generation of *overestimated* fitted DCS values for the π^+p reaction and *underestimated* ones for the CX reaction. It appears that the optimisation of the description of the input data is achieved at the expense of creating a bias in the reproduction of the two subsets (reactions) comprising the set of the input measurements. Equivalently, one might claim that the $I = 3/2$ amplitudes obtained with the model have a difficulty to simultaneously account for the π^+p and CX reactions. As these difficulties were not present in the PSA of the $\pi^\pm p$ elastic-scattering data (at least, at a noticeable level), one may pose the question whether it makes sense to include the CX measurements into a common optimisation scheme, along with data from other reactions.

The distribution of the normalised residuals is shown in Fig. 9, along with the optimal Gaussian function; the χ^2 value of this fit was 25.5 for 22 DOF. The offset \bar{r} (for the definition, see Section 3.4.4 of Ref. [1]) came out equal to $(-6.8 \pm 4.2) \cdot 10^{-2}$. For the sake of completeness, we also give the optimal value and the uncertainty of parameter B of the Gaussian fit to the data: $B = 0.497 \pm 0.038$; the expectation value for B is 0.5.

5.2.4 Reproduction of the π^-p PTCSs

We mentioned in Section 3 of Ref. [1] that, as the nine existing π^-p PTCSs and total-nuclear cross sections contain a component from CX scattering, they could not have been used in our PSA of the elastic-scattering data; we added that the inclusion of these data in any part of that analysis would perplex the discussion on the violation of the isospin invariance in the hadronic part of the πN interaction. The results of the reproduction of the three ⁵ measured PTCSs (where the contributions to the observable may be easily disentangled) are shown in Table 8. We notice that the contributions from the CX reaction are large and substantiate our decision to avoid including these data in the fits to the elastic-scattering measurements.

The measurements of the π^-p PTCS may be compared to the results obtained after summing up the contribution of the π^-p elastic-scattering PTCS and that of the entire CX TCS; this is dictated by the experimental technique employed in these measurements, namely, the detection of only the π^- 's (interacting or passing through) downstream of the target, within a cone of aperture $2\theta_L$ with its apex at the geometrical centre of the target, where θ_L is the laboratory-angle cut associated with the measurement (30° for the three available data points). Regarding the component of the CX TCS, one may use either the prediction from the PSA of the two elastic-scattering reactions [1] or the one obtained from the results of the present work; the better reproduction of the experimental data when invoking the CX TCS of the present work would be in favour of this paper. Although a slight preference for the results of this work has been seen, the experimental uncertainties are too large to lead to definite conclusions.

6 Investigation of the absolute normalisation of the CX data on the basis of the ZUAS12 prediction

We will next investigate the absolute normalisation of the CX data sets using the ZUAS12 prediction as reference. To this end, we must determine the amount at which the reference predictions for each CX data set (i.e., the y_{ij}^{th} values appearing in Eq. (1) of Ref. [1]) must be floated in order to optimally reproduce the experimental data of the specific CX data set (i.e., the y_{ij}^{exp} values). Therefore, relevant in this part of the study are the scale factors for

⁵ Concerning the FRIEDMAN90 measurement [24], we are aware of the revision in the energy calibration of the M11 pion channel at TRIUMF (which took place in the early 1990s), yet we have not found another published value for this measurement; the corrected energy values for the π^+p PTCSs of Ref. [24] appeared a few years after the original publication.

free floating \hat{z}_j , given in Eq. (5) of Ref. [1].

The extracted values of the scale factors \hat{z}_j and their total uncertainties may be found in Table 9 and, plotted separately for the DCS, TCS, AP, and LEC measurements, in Fig. 10. The four FITZGERALD86 data sets which had been freely floated in Section 5.1 are not shown; their \hat{z}_j factors came out equal to 2.03(14), 2.26(15), 2.28(14), and 1.52(13) (the order corresponds to increasing energy). Even when using only the CX data, the scale factors obtained for these data sets (see Table 3) significantly exceed the expectation value of 1. The \hat{z}_j factor of the BREITSCHOPF06 one-point data set which was eliminated in Section 5.1 came out equal to 0.927(50); this data point is also not shown in Fig. 10. One additional data point, the scattering length b_1 of Ref. [17], has not been included in this figure. In principle, one could assign this data point to the DCS set, in which case the outcome would have been consistent with the scale factors for free floating of the ISENHOWER99 10.60 MeV data; nevertheless, only genuine DCS measurements are shown in Fig. 10.

Inspection of Fig. 10 leaves no doubt that, when using the ZUAS12 prediction as reference, the CX scale factors for free floating contain a large amount of fluctuation. As the ZUAS12 prediction is smooth, the fluctuation observed in the figure reflects the scattering of the absolute normalisation of the CX data sets. For instance, the \hat{z}_j value for the FRLEŽ98 data set comes out equal to 1.431(99). This data set lies in between three data sets with considerably smaller \hat{z}_j values, i.e., between the two ISENHOWER99 20.60 MeV data sets and the MEKTEROVIĆ09 33.89 MeV data set. The values of the absolute normalisation of the two neighbouring data sets of DUCLOS73 (22.60 and 32.90 MeV), as well as that of the JIA08 34.37 MeV data set, are compatible with the reference prediction.

Restricting ourselves below 70 MeV, we calculated the weighted average of the \hat{z}_j factors of Table 9 and Fig. 10. The result is that the low-energy CX measurements lie on average $(15.6 \pm 1.4)\%$ above the ZUAS12 predictions ⁶. Naively translated into a relative difference in the CX scattering amplitude, this result would be equivalent to an effect around the 7 – 8% level.

In order to provide some perspective and motivation to research groups which are active in the low-energy πN experimentation, we will now give the predictions obtained on the basis of the ZUAS12 and ZUAS12a solutions in a number of situations. We will investigate the differences in these two prediction sets and identify the kinematical regions which provide fertile ground for distinguishing experimentally between the two sets of values. We commence with the DCSs and TCSs. (The results on the Legendre-expansion coefficients

⁶ The exclusion of the three remaining FITZGERALD86 data sets leaves this result almost intact.

are expected to follow the sensitivity of the DCS.)

The two predictions around the CX DCS minimum are shown in Fig. 11 for $\theta = 0^\circ$. We observe that the two predictions differ; the ZUAS12a prediction exceeds the one obtained on the basis of the ZUAS12 results by about 1.1 MeV. Additionally, the ZUAS12a solution predicts a deeper DCS minimum.

The shapes of the angular distributions of the CX DCS, obtained on the basis of the ZUAS12 and ZUAS12a solutions, are different below and above the s - and p -wave interference minimum. Below the minimum, the ZUAS12a-based DCS systematically exceeds the ZUAS12 predictions, by varying amounts; at 20 MeV, the relative difference (i.e., the difference normalised to the corresponding ZUAS12 values) is 16.5% for $\theta = 0^\circ$ decreasing to 11.3% at $\theta = 180^\circ$; the corresponding numbers for 30 MeV are: 22.1 and 10.4%; finally, at 40 MeV, the relative differences are: 53.8 and 9.4%. Evidently, the relative difference between the two predictions in the forward direction increases as the beam energy approaches the energy of the s - and p -wave interference minimum. Large effects are also seen in the TCS, slightly decreasing with increasing energy, from about 12.2% at 20 MeV, to 11.2% at 30 MeV, and to 10.0% at 40 MeV. A representative plot of the two predictions for the angular distribution of the CX DCS below the s - and p -wave interference minimum is shown in Fig. 12 for 30 MeV.

The picture is slightly different at the high end of the energies: the ZUAS12a result lies below the ZUAS12 prediction in the forward direction. The two predictions cross each other between 40 and 80°; above the crossing, the ZUAS12a prediction exceeds the ZUAS12 one (by smaller amounts when compared to the low energies). At 60 MeV, the relative difference between the two predictions at $\theta = 0^\circ$ is -11.7% , increasing to 7.3% at $\theta = 180^\circ$; at 80 MeV, the values are: -6.7 and 5.2% , whereas at 100 MeV, they are: -6.8 and 3.4% . The net effect in the TCS decreases with increasing energy, from about 7.3% at 60 MeV, to 4.6% at 80 MeV, and to 2.1% at 100 MeV. A representative plot of the two predictions for the angular distribution of the CX DCS above the s - and p -wave interference minimum is shown in Fig. 13 for 80 MeV.

The AP shows high sensitivity to the effect under investigation around the s - and p -wave interference minimum. The few available measurements of the AP in the low-energy CX reaction have been taken at 98.10 and 100.00 MeV, where the differences between the two prediction sets are small.

We finally comment on the experiment of Ref. [20], which took data at forward angles, at six energies around the CX DCS minimum. The authors have made the point that their data ‘show no evidence for unexpected isospin-breaking effects’. To start with, according to Table 3 and assuming the correctness of the absolute normalisation of the bulk of the CX data, the JIA08 measure-

ments lie between 0.5 and 1.5σ (σ , in this case, being equivalent to 10%) below the optimal solution obtained *only* from the CX data in Section 5.1. To investigate the issue further, we generated the ZUAS12 and ZUAS12a predictions, corresponding to the values of the energy and CM scattering angle of these data. As seen in Figs. 14, these two predictions lie close to one another in the kinematical region of the measurements. As a result, the experiment indeed agrees with the ZUAS12 prediction, but it also does with the ZUAS12a prediction (which was not available at the time the report of the experimental group appeared). Given the large normalisation uncertainties of the low-energy πN experiments, as well as the general closeness of the ZUAS12 and ZUAS12a predictions, it is rather unlikely that any single experiment can disprove the violation of the isospin invariance in the hadronic part of the πN interaction, especially one with a normalisation uncertainty at the 10% level.

7 Possible causes of the observed differences between the ZUAS12 and ZUAS12a predictions

We now summarise the main results obtained so far.

- Three of the values of the parameters of the K -matrix parameterisations (i.e., $\tilde{a}_{0+}^{1/2}$, d_{13} , and e_{13}), extracted in the analysis of the tDB $_{+/0}$, differ significantly from those obtained in the analysis of the tDB $_{+/-}$.
- Two of the values of the parameters of the ETH model (i.e., G_ρ and $g_{\pi NN}$), extracted in the analysis of the tDB $_{+/0}$, differ significantly from those obtained in the analysis of the tDB $_{+/-}$.
- When using the ETH model, the substitution of the tDB $_-$ with the tDB $_0$ leads to noticeable deterioration of the results of the fits, indicating difficulties in the description of these measurements on the basis of *one* set of parameter values of the ETH model. In this respect, the results of Table 6, for the three values of p_{min} which have been used in Ref. [1], are consistent.
- A significant difference has been seen in the s -wave phase shift $\tilde{\delta}_{0+}^{1/2}$; smaller differences are observed in two p -wave phase shifts, i.e., in $\tilde{\delta}_{1+}^{3/2}$ and in $\tilde{\delta}_{1-}^{1/2}$.
- The reproduction of the absolute normalisation of the CX data sets on the basis of the ZUAS12 prediction is poor below 70 MeV. The differences observed amount to a 7 – 8% effect in the CX scattering amplitude.

These differences between the ZUAS12 and ZUAS12a solutions and the predictions obtained on their basis are significant. We will now attempt to identify possible causes of the observed discrepancies.

In view of the results obtained so far, there are three assumptions, of which at most two can be simultaneously valid.

- The absolute normalisation of the bulk of the low-energy πN experimental data is reliable.
- The residual contributions in the em corrections, applied to the experimental data in order to extract the hadronic part of the πN amplitude, are negligible.
- The isospin invariance in the hadronic part of the πN interaction holds.

We will next elaborate on each of the three possibilities arising from the non-fulfillment of the aforementioned presumptions.

7.1 *Experimental problems*

The first explanation for the observed differences involves a trivial effect, namely the systematic incorrectness of the absolute normalisation in the low-energy πN data. Arguments have been presented in Ref. [7], to substantiate the claim that some of the reported uncertainties in the πN experimentation have been underestimated; concerning this last issue, the data analysis dictates that the two elastic-scattering reactions are more affected than the CX.

Our first point concerns the statistical uncertainties of the data points. When visually inspecting the low-energy πN data, one is frequently unable to comprehend how it is possible for successive measurements (i.e., at neighbouring values of the CM scattering angle) to be so different. There are many occasions in the databases where the statistical uncertainties of the data points seem questionable.

Our second point concerns the systematic effects. It is not understood how the absolute normalisation of some experiments, e.g., of the FITZGERALD86 data sets at the three lowest energies, may be wrong (according to the bulk of the tDB₀) by an average of about 70% (and of a fourth data set by 45%), at a time when the reported normalisation uncertainty in the experiment was 7.8%. Such an effect may only be caused by any of three reasons (or their combination): a) the determination of the absolute normalisation in the experiment had been erroneous, b) the energy of the incoming beam had not been what the experimenters expected, or c) the normalisation uncertainty in the experiment had been grossly underestimated.

Our third point concerns the small values of the normalisation uncertainty reported in many low-energy πN experiments; for instance, the reported normalisation uncertainties in 37 out of the 90 data sets in the initial DB_{+/-}

are below 3%. One could possibly try to modify the small values of the normalisation uncertainty (perhaps, by setting a lower limit at 3%), yet such an approach seems arbitrary. Consequently, one is left with no other option than to rely on an approach which places importance on the absolute normalisation of the bulk of the experimental data and to apply a reasonable procedure for the elimination of the outliers; this is the approach which we set up in Refs. [1,2,7].

There is one disturbing discrepancy in the entire analysis of the $t\text{DB}_{+/-}$ which cannot be easily put aside, namely, the disagreement between the \tilde{a}^{cc} value obtained as an extrapolation from the experimental data (above the πN threshold) and the one extracted directly at the πN threshold from the strong shift of the $1s$ level in pionic hydrogen. Assuming the correctness of both the absolute normalisation of the bulk of the elastic-scattering databases and of the raw measurement of ϵ_{1s} [17], the two extracted values should be compatible, if a consistent set of em corrections (i.e., corrections which have been obtained within the same framework and which are also complete in the sense of containing the contributions from all relevant physical effects) have been applied to the raw data. In case of important residual effects in the em corrections (see next section), the question surfaces as to the energy dependence of these contributions.

7.2 *Residual contributions in the em corrections*

Although it is not clear how these contributions can modify so drastically the overall picture and especially the results of Table 6 (any residual em contributions are expected to affect equally the description of the experimental data on the basis of the K -matrix parameterisations and of the ETH model), the completeness of the em corrections in the πN system at low energies is an important issue which must be properly defined and treated. In Refs. [7,22], some details are given on the effects which the stage-II em corrections contain; these effects are mostly related to the use of the physical instead of the (unknown) hadronic masses for the proton, the neutron, and the charged and neutral pion in the determination of the em corrections [26,27]. On the other hand, it may be argued that the appropriate inclusion of these effects should lead to the optimal description of the input data. If this is the case, then the iterative procedure which had been set forth in the determination of the em corrections in Refs. [26,27] must have captured some of these effects. Unable, however, to either validate this statement or refute it, we can only encourage the theoretical re-assessment of the role of the em effects in the low-energy πN interaction.

7.3 *The violation of the isospin invariance in the hadronic part of the πN interaction*

This is the last of the options which may be put forth in an attempt to explain the observed discrepancies and, admittedly, the most interesting one in Physics terms. This possibility may account for the results of Table 6. There has been a great amount of discussion regarding the acceptance of the conclusions of Refs. [4,5]. One is tempted, however, to pose the question: ‘Why should the isospin invariance in the πN system be obeyed in the first place?’ After all, the hadronic masses of the u and d quarks are different; similarly, the masses of the nucleons differ (beyond trivial em effects), and so do those of the Δ ’s. It appears, therefore, that the appropriate question to ask is not whether the isospin invariance is violated, but at which amount it is. Within the framework of the heavy-baryon Chiral-Perturbation Theory, the group of Meißner have repeatedly treated isospin-breaking effects in the πN system at low energies and concluded that the discrepancy should be at most at the percent level (e.g., see Ref. [28] and the references cited therein).

Two mechanisms had been proposed in the past, to account for the violation of the isospin invariance in the hadronic part of the πN interaction at the level of Feynman graphs: the first mechanism affects the elastic scattering ($\rho^0 - \omega$ mixing [29]-[31]), the second the CX reaction ($\eta - \pi^0$ mixing [32]). As both the ω and the η states are singlets, the coupling of the former to the ρ^0 and of the latter to the π^0 explicitly violate the isospin invariance. Given that, in the case of the elastic scattering, only one graph (i.e., the t -channel ρ -exchange graph) is affected, whereas in the case of the CX reaction all graphs are influenced (see Fig. 15), one would be prone to conclude that the isospin-breaking effects are more important in the latter case; however, Ref. [32] concluded with the statement that ‘...the isospin violation from $\eta - \pi^0$ mixing can be safely ignored in πN partial-wave analyses.’ In fact, the possibility of large isospin-breaking effects in specific kinematical regions is not refuted in Ref. [32]; for instance, emphasis in that paper was placed on the effects induced in the amplitude of one higher baryon resonance, which were expected to be around the 7% level. Unfortunately, there is no indication that the kinematical region around the πN threshold received equal attention in Ref. [32]. Of course, this is not very surprising given the scarcity of the low-energy πN measurements around the time Ref. [32] appeared; in fact, below $T = 100$ MeV, the only CX DCS measurements, which were available at that time, were the 3 data points of Ref. [9].

We noticed that the coupling constant $g_{\pi NN}$ is significantly affected when substituting the tDB₋ with the tDB₀. Of course, if the isospin invariance is violated, there is not *one* coupling constant $g_{\pi NN}$; one must distinguish between $g_{\pi^0 pp}$, $g_{\pi^0 nn}$, and $g_{\pi^\pm pn}$. In this case, the fits to the elastic-scattering

data essentially determine $g_{\pi^\pm pn}$, whereas those involving the CX reaction also contain contributions from $g_{\pi^0 pp}$ and $g_{\pi^0 nn}$. As a result, the value of the coupling constant $g_{\pi NN}$ extracted from the common fits to the tDB_{+/0} represents a weighted average of these three quantities. The differences observed imply that at least one of the two $g_{\pi^0 NN}$ coupling constants differs from $g_{\pi^\pm pn}$. The isospin-breaking effects on $g_{\pi NN}$ have been studied theoretically and generally found to be small; for instance, Ref. [33] evaluated these effects using QCD sum rules and reported that $g_{\pi^\pm pn}$ should be equal to the average of the two $g_{\pi^0 NN}$ values and that the splitting should be expected between 1.2 and 3.7%. The difference between the two $g_{\pi NN}$ values of Table 4 is larger, around the 4.5% level.

8 Discussion and Summary

This study concludes the analysis of the presently-available pion-nucleon (πN) data below pion laboratory kinetic energy of 100 MeV. The separate analysis of the data for the two elastic-scattering and for the charge-exchange (CX) reactions was enabled via suitable parameterisations of the s - and p -wave K -matrix elements at low energies. Common fits to the data were performed using either these K -matrix parameterisations or the ETH model of Ref. [6], which is based on meson-exchange t -channel graphs, as well as on the s - and u -channel N and Δ contributions. The analysis with the K -matrix parameterisations led to the identification of the outliers in the databases and tested the self-consistency of the input prior to its submission to the fits using the ETH model. The optimal values of the model parameters, as well as their correlation matrix, were obtained from the ensuing fits and were used as the basis for generating Monte-Carlo predictions for the em-modified hadronic phase shifts, for the low-energy πN constants, as well as for the standard observables (i.e., for the differential cross section (DCS), analysing power (AP), partial-total cross section (PTCS), and total cross section (TCS)) for any of the three reactions, at any value of the relevant kinematical variables (i.e., energy and scattering angle for the DCS and AP, energy and laboratory-angle cut for the PTCS, and energy for the TCS).

Given that the electromagnetic (em) corrections (which are applied to the hadronic phase shifts in order to extract the πN partial-wave amplitudes, which, in turn, lead to the observables) of Refs. [26,27] have been obtained by using the physical, instead of the (unknown) hadronic, masses for the proton, the neutron, and the charged and neutral pion, we have assumed the cautious attitude of considering the various physical quantities (i.e., the model parameters, the low-energy πN constants, the hadronic phase shifts, etc.) not purely hadronic, but em-modified hadronic. At the present time, one cannot assess the importance of the residual em effects (i.e., of the stage-II em corrections).

Following the procedure described in the first paragraph of the present section, we first analysed the two elastic-scattering reactions and obtained the solution for the model parameters, as well as the predictions for the em-modified hadronic phase shifts derived on their basis [1]. In this paper, we analysed the π^+p and CX databases. By comparing the results of these two PSAs, large effects were found both in two of the model parameters, as well as in the em-modified hadronic phase shifts $\tilde{\delta}_{0+}^{1/2}$; significantly smaller differences have been found in two p -wave phase shifts.

Assuming the correctness of the absolute normalisation of the bulk of the low-energy πN databases, as well as the negligibility of the residual contributions in the em corrections (i.e., of the stage-II effects), these discrepancies can only be attributed to the violation of the isospin invariance in the hadronic part of the πN interaction at low energies. The effect observed is at the level of 7 – 8% in the scattering amplitude below 70 MeV.

The results of this study agree well with those obtained in the mid 1990s, when the isospin invariance in the πN system was first tested by using the then-available experimental information. This agreement is notable given the changes of the databases in the meantime (e.g., the CX database has been enlarged by a factor of seven), the analysis methods, and the em corrections applied to the input data. Our result is in disagreement with predictions (for the isospin-breaking effect in the CX scattering amplitude) obtained within the framework of the heavy-baryon Chiral-Perturbation Theory, according to which, the expected effects should be around the percent level.

There are a number of directions which could next be pursued. a) Extensive modifications in our database structure and analysis software should be made in order to include in the fits the AP measurements of Ref. [34] and produce a new phase-shift solution from the elastic-scattering reactions. Given the goodness of the reproduction of these data with our ZUAS12 prediction (see Section 3.4.5 of Ref. [1]), only small differences are expected. b) It might be helpful to include in the (so-far isospin-invariant) ETH model the isospin-violating Feynman graphs of Fig. 15 (as well as the corresponding $\rho^0 - \omega$ graph for elastic scattering), fixing the coupling constants and masses from the literature. With the added contributions, one could subsequently investigate whether a significant improvement can be obtained in the description of the πN data at low energies. If the graphs of Fig. 15 are the dominant ones and if the effects observed in the present study are indeed due to the violation of the isospin invariance, then the description of the experimental data (especially when the CX reaction is included in the fits) should improve significantly. c) The extrapolation of the amplitudes of the ETH model in the unphysical region, to the Cheng-Dashen point (in order to obtain reliable values of the πN Σ -term), should be seriously investigated.

Finally, it would be interesting to investigate the violation of the isospin invariance using only the results from pionic hydrogen and deuterium (i.e., the data acquired directly at the πN threshold) by extracting and comparing the scattering lengths and their standard combinations, in a way similar to the one introduced in Ref. [35]. The results of the original experiments (which were performed in the 1990s) are known, as are those for pionic deuterium of the successor experiment; the results of this experiment for pionic hydrogen are still marked as preliminary [36]. It would be interesting to compare all these pieces of information and investigate how they match the picture which is slowly emerging for the πN system at low energies. The findings of the present work, which corroborate the conclusions of Refs. [4,5], suggest modifications (at least at the low energies) in the established formalism used in the analysis of the πN data (e.g., in dispersion-relation schemes). Additionally, the extrapolation of the πN partial-wave amplitudes in the unphysical region, to the Cheng-Dashen point, must consequently be reconsidered.

Acknowledgements

We acknowledge helpful discussions with W.R. Gibbs. We are grateful to T.P. Gorringer for communicating to us the measurements of Ref. [20]. We dedicate this work to W.S. Woolcock (1934-2012) who collaborated with us until the end of 2011. He influenced this analysis during its early stages with many important comments and suggestions. Quite unexpectedly, in September 2012, he died after a short illness.

Figure 15 has been drawn with the software package JaxoDraw [37], available from <http://jaxodraw.sourceforge.net/>.

References

- [1] E. Matsinos, G. Rasche, *J. Mod. Phys.* 3 (2012) 1369-87.
- [2] E. Matsinos, G. Rasche, *Nucl. Phys. A* 903 (2013) 65-80.
- [3] H. Denz et al., *Phys. Lett. B* 633 (2006) 209-13.
- [4] W.R. Gibbs, Li Ai, W.B. Kaufmann, *Phys. Rev. Lett.* 74 (1995) 3740-3.
- [5] E. Matsinos, *Phys. Rev. C* 56 (1997) 3014-25.
- [6] P.F.A. Goudsmit, H.J. Leisi, E. Matsinos, B.L. Birbrair, A.B. Gridnev, *Nucl. Phys. A* 575 (1994) 673-706.

- [7] E. Matsinos, W.S. Woolcock, G.C. Oades, G. Rasche, A. Gashi, Nucl. Phys. A 778 (2006) 95-123.
- [8] D.V. Bugg et al., Nucl. Phys. B 26 (1971) 588-96.
- [9] J. Duclos et al., Phys. Lett. B 43 (1973) 245-8.
- [10] M. Salomon, D.F. Measday, J-M. Poutissou, B.C. Robertson, Nucl. Phys. A 414 (1984) 493-507.
- [11] D.H. Fitzgerald et al., Phys. Rev. C 34 (1986) 619-26.
- [12] A. Bagheri et al., Phys. Rev. C 38 (1988) 885-94.
- [13] J.C. Staško, Ph.D. dissertation, University of New Mexico, 1993.
- [14] E. Frlež et al., Phys. Rev. C 57 (1998) 3144-52.
- [15] C.V. Gaulard et al., Phys. Rev. C 60 (1999) 024604.
- [16] L.D. Isenhower et al., πN Newsletter 15 (1999) 292-5.
- [17] H.-Ch. Schröder et al., Eur. Phys. J. C 21 (2001) 473-88.
- [18] M.E. Sadler et al., Phys. Rev. C 69 (2004) 055206.
- [19] J. Breitschopf et al., Phys. Lett. B 639 (2006) 424-8.
- [20] Y. Jia et al., Phys. Rev. Lett. 101 (2008) 102301.
- [21] D. Mekterović et al., Phys. Rev. C 80 (2009) 055207.
- [22] G.C. Oades, G. Rasche, W.S. Woolcock, E. Matsinos, A. Gashi, Nucl. Phys. A 794 (2007) 73-86.
- [23] R.A. Arndt, W.J. Briscoe, I.I. Strakovsky, R.L. Workman, Phys. Rev. C 74 (2006) 045205; SAID PSA Tool, <http://gwdac.phys.gwu.edu>.
- [24] E. Friedman et al., Nucl. Phys. A 514 (1990) 601-12.
- [25] B.J. Kriss et al., Phys. Rev. C 59 (1999) 1480-7.
- [26] A. Gashi, E. Matsinos, G.C. Oades, G. Rasche, W.S. Woolcock, Nucl. Phys. A 686 (2001) 447-62.
- [27] A. Gashi, E. Matsinos, G.C. Oades, G. Rasche, W.S. Woolcock, Nucl. Phys. A 686 (2001) 463-77.
- [28] M. Hoferichter, B. Kubis, Ulf-G. Meißner, Phys. Lett. B 678 (2009) 65-71.
- [29] S.A. Coon, R.C. Barrett, Phys. Rev. C 36 (1987) 2189-94.
- [30] T. Goldman, J.A. Henderson, A.W. Thomas, Few-Body Syst. 12 (1992) 123-32.
- [31] G.A. Miller, Chin. J. Phys. 32 (1994) 1075-87.
- [32] R.E. Cutkosky, Phys. Lett. B 88 (1979) 339-42.

- [33] T. Meissner, E.M. Henley, Phys. Rev. C 55 (1997) 3093-9.
- [34] R. Meier et al., Phys. Lett. B 588 (2004) 155-62.
- [35] H.J. Leisi et al., ‘Is isospin symmetry violated in the pion-nucleon sector at threshold?’, in *Chiral Dynamics: Theory and Experiment, Proceedings of the Workshop Held at MIT*, Cambridge, MA, USA, 25-29 July 1994, eds. A.M. Bernstein and B.R. Holstein, Springer, Berlin, 1995, pp. 241-43.
- [36] D. Gotta, private communication; see also <http://www2.fz-juelich.de/ikp/exotic-atoms/index.php>.
- [37] D. Binosi, L. Theußl, ‘JaxoDraw: A graphical user interface for drawing Feynman diagrams’, Comput. Phys. Commun. 161 (2004) 76-86.

Table 1

The low-energy CX experiments in chronological order. The first column contains a label identifying the experiment. Columns 2 – 5 contain the number of data points reported in each experiment: DCS stands for the differential cross section, LEC for the first three coefficients in the Legendre expansion of the DCS, TCS for the total cross section, and AP for the analysing power. The adjacent column contains the pion laboratory kinetic energy or energy range of the experiment. The CM scattering angle or angular interval of the measurements is listed in the last column. The experiment of Ref. [17] obtained the scattering length \tilde{a}^{c0} ($= \sqrt{2}b_1$) from a measurement of the width of the $1s$ state of pionic hydrogen; therefore, it cannot be placed in any of the categories under Columns 2 – 5.

Experiment	DCS	LEC	TCS	AP	T (MeV)	θ
BUGG71 [8]			1		90.90	
DUCLOS73 [9]	3				22.60 – 42.60	180°
SALOMON84 [10]		6			27.40, 39.30	
FITZGERALD86 [11]	21				32.48 – 63.21	9.60 – 25.04°
BAGHERI88 [12]		12			45.60 – 91.70	
STAŠKO93 [13]				4	100.00	75.00 – 130.00°
FRLEŽ98 [14]	6				27.50	4.70 – 50.90°
GAULARD99 [15]				6	98.10	8.02 – 86.05°
ISENHOWER99 [16]	40				10.60 – 39.40	9.60 – 168.24°
SCHROEDER01 [17]					0.00	
SADLER04 [18]	60				63.86 – 94.57	18.19 – 161.81°
BREITSCHOPF06 [19]			9		38.90 – 96.50	
JIA08 [20]	24				34.37 – 59.68	5.81 – 41.39°
MEKTEROVIĆ09 [21]	140				33.89 – 86.62	18.19 – 161.81°

Table 2

The list of outliers in the CX database. The rows represent steps in the outlier-identification/elimination process. The columns indicate: the χ^2 value, the number of degrees of freedom in the fit, and the action which had to be taken at the specific step. No data was marked for removal at step 6.

Step	χ^2	NDF	Action
1	400.3	326	Freely float FITZGERALD86 at 40.26 MeV
2	375.1	325	Freely float FITZGERALD86 at 36.11 MeV
3	351.5	324	Freely float FITZGERALD86 at 32.48 MeV
4	333.4	323	Exclude BREITSCHOPF06 at 75.10 MeV
5	324.5	322	Freely float FITZGERALD86 at 47.93 MeV
6	312.8	321	

Table 3

The data sets comprising the truncated database for the CX reaction, the pion laboratory kinetic energy, the number of degrees of freedom for each data set, the scale factor z_j which minimises χ_j^2 (Eq. (1) of Ref. [1]), the values of $(\chi_j^2)_{min}$, and the p-value associated with the description of each data set. The numbers of this table correspond to the final fit to the data using the K -matrix parameterisations (see Section 5.1). In the case of the freely-floated data sets, the scale factor z_j is identical to \hat{z}_j of Eq.(5) of Ref. [1].

Data set	T (MeV)	(NDF) $_j$	z_j	$(\chi_j^2)_{min}$	p-value	Comments
BUGG71	90.90	1	1.0225	0.1470	0.7014	
DUCLOS73	22.60	1	0.9413	1.2465	0.2642	
DUCLOS73	32.90	1	0.9717	0.2700	0.6033	
DUCLOS73	42.60	1	0.9098	2.3836	0.1226	
SALOMON84	27.40	3	0.9720	2.8685	0.4124	
SALOMON84	39.30	3	0.9937	1.0774	0.7825	
FITZGERALD86	32.48	2	1.5076	2.3635	0.3067	freely floated
FITZGERALD86	36.11	2	1.7103	1.1845	0.5531	freely floated
FITZGERALD86	40.26	2	1.8274	6.1362	0.0465	freely floated
FITZGERALD86	47.93	2	1.4497	1.5402	0.4630	freely floated
FITZGERALD86	51.78	3	1.1236	7.3728	0.0609	
FITZGERALD86	55.58	3	1.0926	2.5611	0.4644	
FITZGERALD86	63.21	3	1.0503	1.2246	0.7471	
BAGHERI88	45.60	3	1.0056	0.1314	0.9878	
BAGHERI88	62.20	3	0.9589	3.4999	0.3208	
BAGHERI88	76.40	3	0.9731	3.2706	0.3518	
BAGHERI88	91.70	3	1.0151	2.8032	0.4230	
STAŠKO93	100.00	4	0.9948	1.4336	0.8383	
FRLEŽ98	27.50	6	1.0902	10.2313	0.1152	
GAULARD99	98.10	6	1.0241	1.1007	0.9815	
ISENHOWER99	10.60	4	1.0203	2.1816	0.7024	
ISENHOWER99	10.60	5	1.0054	1.4611	0.9175	
ISENHOWER99	10.60	6	1.0181	8.0844	0.2320	
ISENHOWER99	20.60	5	0.9803	1.5435	0.9080	
ISENHOWER99	20.60	6	1.0120	8.1813	0.2251	

Table 3 continued

Data set	T (MeV)	$(\text{NDF})_j$	z_j	$(\chi_j^2)_{\min}$	p-value	Comments
ISENHOWER99	39.40	4	1.0701	7.1132	0.1300	
ISENHOWER99	39.40	5	1.0597	8.4184	0.1346	
ISENHOWER99	39.40	5	0.9514	5.1617	0.3965	
SCHROEDER01	0.00	1	0.9747	2.5184	0.1125	
SADLER04	63.86	20	0.9548	16.0803	0.7116	
SADLER04	83.49	20	0.9881	11.6506	0.9276	
SADLER04	94.57	20	1.0296	7.2573	0.9958	
BREITSCHOPF06	38.90	1	0.9960	0.1643	0.6852	
BREITSCHOPF06	43.00	1	1.0011	0.0259	0.8721	
BREITSCHOPF06	47.10	1	0.9981	0.0572	0.8110	
BREITSCHOPF06	55.60	1	0.9952	0.2074	0.6488	
BREITSCHOPF06	64.30	1	0.9725	3.7739	0.0521	
BREITSCHOPF06	65.90	1	0.9779	2.3441	0.1258	
BREITSCHOPF06	76.10	1	0.9814	1.6114	0.2043	
BREITSCHOPF06	96.50	1	0.9816	0.6152	0.4328	
JIA08	34.37	4	0.8434	4.9306	0.2945	
JIA08	39.95	4	0.8680	3.1715	0.5295	
JIA08	43.39	4	0.8777	2.5167	0.6416	
JIA08	46.99	4	0.9798	5.1175	0.2754	
JIA08	54.19	4	0.9080	2.0430	0.7279	
JIA08	59.68	4	0.9265	3.2449	0.5177	
MEKTEROVIĆ09	33.89	20	1.0239	17.0075	0.6525	
MEKTEROVIĆ09	39.38	20	1.0145	14.7514	0.7905	
MEKTEROVIĆ09	44.49	20	1.0100	33.1457	0.0325	
MEKTEROVIĆ09	51.16	20	1.0357	15.0473	0.7737	
MEKTEROVIĆ09	57.41	20	1.0394	19.9034	0.4640	
MEKTEROVIĆ09	66.79	20	1.0235	19.4707	0.4914	
MEKTEROVIĆ09	86.62	20	1.0019	31.1877	0.0528	

Table 4

The values of the seven parameters of the ETH model obtained from the common fit to the truncated π^+p and CX databases (ZUAS12a solution). The ZUAS12 solution [1], obtained from the PSA of the $\pi^\pm p$ elastic-scattering data for $p_{min} \approx 1.24 \cdot 10^{-2}$, is shown for comparison.

	This work (ZUAS12a)	ZUAS12
$G_\sigma(GeV^{-2})$	30.0 ± 2.0	27.48 ± 0.86
K_σ	0.150 ± 0.058	0.016 ± 0.034
$G_\rho(GeV^{-2})$	59.26 ± 0.58	54.67 ± 0.61
K_ρ	1.65 ± 0.24	0.66 ± 0.41
$g_{\pi NN}$	13.43 ± 0.11	12.84 ± 0.12
$g_{\pi N\Delta}$	28.97 ± 0.29	29.77 ± 0.26
Z	-0.353 ± 0.098	-0.552 ± 0.056

Table 5

The correlation (Hessian) matrix for the seven parameters of the ETH model for the common fit to the truncated π^+p and CX databases.

	G_σ	K_σ	G_ρ	K_ρ	$g_{\pi NN}$	$g_{\pi N\Delta}$	Z
G_σ	1.0000	0.4625	0.1180	0.3231	0.3884	-0.5044	-0.2165
K_σ	0.4625	1.0000	0.7696	0.8870	0.8424	-0.9461	0.7475
G_ρ	0.1180	0.7696	1.0000	0.7081	0.8395	-0.7573	0.7959
K_ρ	0.3231	0.8870	0.7081	1.0000	0.7794	-0.8712	0.7274
$g_{\pi NN}$	0.3884	0.8424	0.8395	0.7794	1.0000	-0.9053	0.6340
$g_{\pi N\Delta}$	-0.5044	-0.9461	-0.7573	-0.8712	-0.9053	1.0000	-0.6435
Z	-0.2165	0.7475	0.7959	0.7274	0.6340	-0.6435	1.0000

Table 6

The various χ^2 values obtained in the analysis of the low-energy πN data, along with the number of degrees of freedom in each fit, for three values of p_{min} (the confidence level in the statistical tests); these three p_{min} values correspond to 3, 2.5, and 2σ effects in the normal distribution. The definitions of the databases are given at the end of Section 2. Separate fits to the three databases using the ETH model have not been attempted, due to the largeness of the correlations among the model parameters in that case. It must be mentioned that some of the χ^2 values of this table, categorised under Ref. [1], have not explicitly appeared in that paper.

Parametric model	tDB ₊ [1]	tDB ₋ [1]	tDB ₀ (this work)	tDB _{+/-} [1]	tDB _{+/0} (this work)
$p_{min} \approx 2.70 \cdot 10^{-3} (3\sigma)$					
<i>K</i> -matrix	434.4/334	397.9/325	333.4/323	825.9/659	765.1/657
ETH model	–	–	–	905.4/666	994.4/664
$p_{min} \approx 1.24 \cdot 10^{-2} (2.5\sigma)$					
<i>K</i> -matrix	427.2/333	371.0/321	312.8/321	792.4/654	737.0/654
ETH model	–	–	–	872.9/661	960.5/661
$p_{min} \approx 4.55 \cdot 10^{-2} (2\sigma)$					
<i>K</i> -matrix	357.0/310	332.3/316	306.4/320	684.4/626	663.3/630
ETH model	–	–	–	755.2/633	842.7/637

Table 7

The values of the six s - and p -wave em-modified hadronic phase shifts (in degrees), obtained on the basis of the results of Tables 4 (ZUAS12a solution) and 5.

T (MeV)	$\tilde{\delta}_{0+}^{3/2}$ (S31)	$\tilde{\delta}_{0+}^{1/2}$ (S11)	$\tilde{\delta}_{1+}^{3/2}$ (P33)	$\tilde{\delta}_{1-}^{3/2}$ (P31)	$\tilde{\delta}_{1+}^{1/2}$ (P13)	$\tilde{\delta}_{1-}^{1/2}$ (P11)
20	-2.455(52)	4.535(62)	1.3286(91)	-0.2416(81)	-0.1710(70)	-0.410(12)
25	-2.860(54)	5.056(66)	1.884(12)	-0.332(11)	-0.2316(99)	-0.540(17)
30	-3.259(56)	5.519(70)	2.515(15)	-0.430(15)	-0.295(13)	-0.670(23)
35	-3.657(57)	5.937(72)	3.222(18)	-0.534(19)	-0.360(17)	-0.795(29)
40	-4.055(58)	6.318(75)	4.007(20)	-0.643(24)	-0.427(21)	-0.914(35)
45	-4.455(59)	6.666(78)	4.873(22)	-0.756(29)	-0.495(25)	-1.023(42)
50	-4.858(61)	6.987(82)	5.824(24)	-0.874(34)	-0.562(29)	-1.123(49)
55	-5.264(64)	7.282(87)	6.865(26)	-0.994(40)	-0.630(34)	-1.211(57)
60	-5.673(69)	7.554(93)	8.000(28)	-1.118(46)	-0.697(39)	-1.287(65)
65	-6.087(75)	7.80(10)	9.238(30)	-1.245(52)	-0.763(44)	-1.350(74)
70	-6.504(82)	8.04(11)	10.586(34)	-1.374(59)	-0.828(50)	-1.398(83)
75	-6.924(92)	8.25(12)	12.053(39)	-1.506(67)	-0.893(56)	-1.431(92)
80	-7.35(10)	8.44(13)	13.648(47)	-1.640(74)	-0.956(62)	-1.45(10)
85	-7.78(11)	8.62(14)	15.383(57)	-1.775(82)	-1.017(68)	-1.45(11)
90	-8.21(13)	8.78(16)	17.268(70)	-1.912(90)	-1.078(75)	-1.43(12)
95	-8.64(14)	8.93(17)	19.318(85)	-2.051(99)	-1.136(82)	-1.40(14)
100	-9.08(16)	9.06(19)	21.54(10)	-2.19(11)	-1.193(89)	-1.35(15)

Table 8

Reproduction of the π^-p PTCSs which had not been used in Ref. [1]. The first four columns correspond to a label identifying the measurement, the pion laboratory kinetic energy, the laboratory-angle cut (θ_L), and the PTCS measurement. The three adjacent columns contain the predictions obtained on the basis of our two PSAs, namely of Ref. [1] and of the present work. The column marked as ' σ_{EL} ' contains the prediction for the π^-p elastic-scattering PTCS (for the particular θ_L value) obtained from the ZUAS12 solution of Ref. [1]. The next column contains the prediction for the CX TCS also obtained from the ZUAS12 solution of Ref. [1]. The last column contains the prediction for the CX TCS obtained from the solution of the present work.

Data point	T (MeV)	θ_L (deg)	σ (mb)	σ_{EL} (mb) [1]	σ_{CX} (mb) [1]	σ_{CX} (mb)
FRIEDMAN90 [24]	50.00	30.00	8.5 ± 0.6	2.15 ± 0.13	6.089 ± 0.048	6.618 ± 0.050
KRISS97 [25]	80.00	30.00	14.6 ± 0.6	2.958 ± 0.076	11.290 ± 0.074	11.808 ± 0.089
KRISS97 [25]	99.20	30.00	23.4 ± 1.1	4.594 ± 0.040	17.34 ± 0.15	17.72 ± 0.17

Table 9

The scale factors \hat{z}_j of the CX data sets, which are appropriate for testing their absolute normalisation relative to the ZUAS12 predictions [1], listed separately for the differential cross sections (upper part), total cross sections (second part), analysing powers (third part), and the results for the coefficients of the Legendre expansion of the differential cross section (last part). The four FITZGERALD86 data sets which had been floated freely in Section 5.1 have not been included. Not listed in the table is also the result of Ref. [17] for the isovector scattering length b_1 . The quantity $\Delta\hat{z}_j$ is the total uncertainty (see end of Section 2.2 of Ref. [1]).

Data set	T (MeV)	\hat{z}_j	$\Delta\hat{z}_j$
DUCLOS73	22.60	1.03	0.14
DUCLOS73	32.90	1.09	0.13
DUCLOS73	42.60	0.95	0.12
FITZGERALD86	51.78	1.29	0.10
FITZGERALD86	55.58	1.250	0.099
FITZGERALD86	63.21	1.203	0.093
FRLEŽ98	27.50	1.431	0.099
ISENHOWER99	10.60	1.45	0.12
ISENHOWER99	10.60	1.331	0.081
ISENHOWER99	10.60	1.307	0.057
ISENHOWER99	20.60	1.205	0.052
ISENHOWER99	20.60	1.229	0.047
ISENHOWER99	39.40	1.48	0.11
ISENHOWER99	39.40	1.245	0.045
ISENHOWER99	39.40	1.089	0.042
SADLER04	63.86	1.050	0.068
SADLER04	83.49	1.045	0.053
SADLER04	94.57	1.063	0.047
JIA08	34.37	1.04	0.12
JIA08	39.95	1.00	0.12
JIA08	43.39	0.94	0.13
JIA08	46.99	1.09	0.14
JIA08	54.19	0.94	0.13
JIA08	59.68	0.99	0.12

Table 9 continued

Data set	T (MeV)	\hat{z}_j	$\Delta\hat{z}_j$
MEKTEROVIĆ09	33.89	1.213	0.040
MEKTEROVIĆ09	39.38	1.182	0.032
MEKTEROVIĆ09	44.49	1.160	0.031
MEKTEROVIĆ09	51.16	1.181	0.033
MEKTEROVIĆ09	57.41	1.167	0.031
MEKTEROVIĆ09	66.79	1.127	0.032
MEKTEROVIĆ09	86.62	1.056	0.030
BUGG71	90.90	1.068	0.061
BREITSCHOPF06	38.90	1.12	0.10
BREITSCHOPF06	43.00	1.17	0.15
BREITSCHOPF06	47.10	1.11	0.12
BREITSCHOPF06	55.60	1.077	0.093
BREITSCHOPF06	64.30	0.967	0.069
BREITSCHOPF06	65.90	0.995	0.067
BREITSCHOPF06	76.10	0.994	0.065
BREITSCHOPF06	96.50	0.999	0.039
STAŠKO93	100.00	0.91	0.11
GAULARD99	98.10	0.962	0.058
SALOMON84	27.40	1.098	0.056
SALOMON84	39.30	1.131	0.059
BAGHERI88	45.60	1.149	0.036
BAGHERI88	62.20	1.042	0.039
BAGHERI88	76.40	1.038	0.036
BAGHERI88	91.70	1.063	0.039

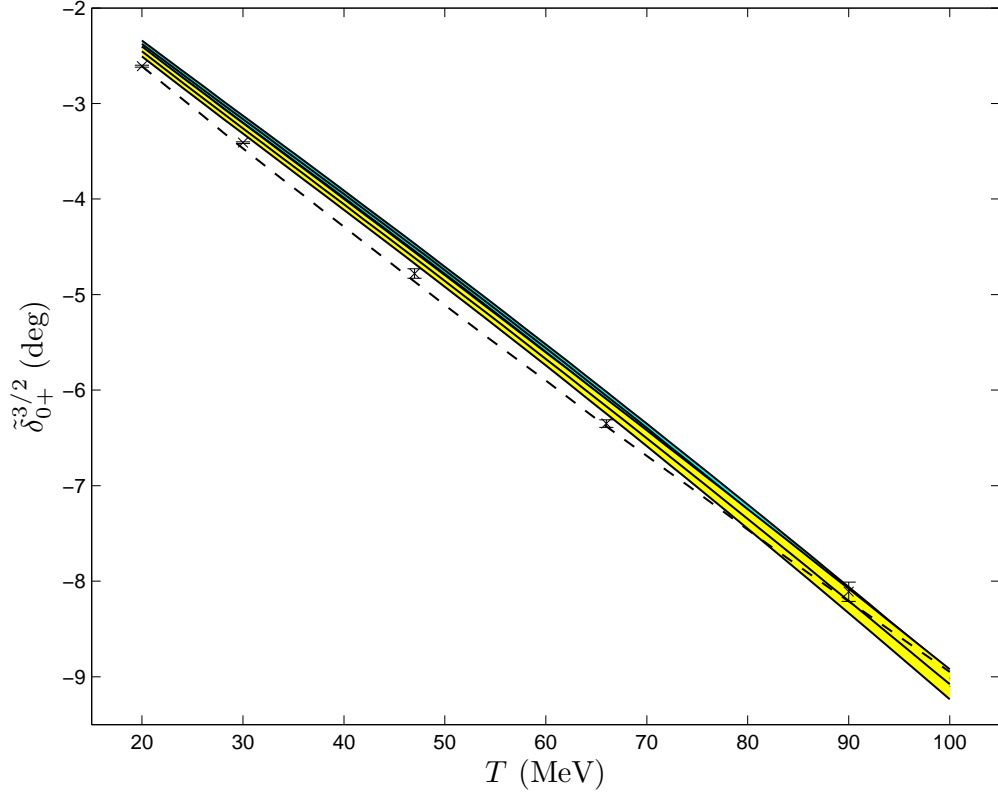


Fig. 1. The energy dependence of the em-modified hadronic phase shift $\tilde{\delta}_{0+}^{3/2}$ (S31) from the present work, along with 1σ uncertainties (yellow band). Also included is the ZUAS12 prediction [1], obtained on the basis of the elastic-scattering data below 100 MeV, along with the corresponding 1σ uncertainties (blue band). The current SAID solution (WI08) [23] is represented by the dashed curve; the five points shown (at $T = 20, 30, 47, 66,$ and 90 MeV) are the single-energy WI08 values.

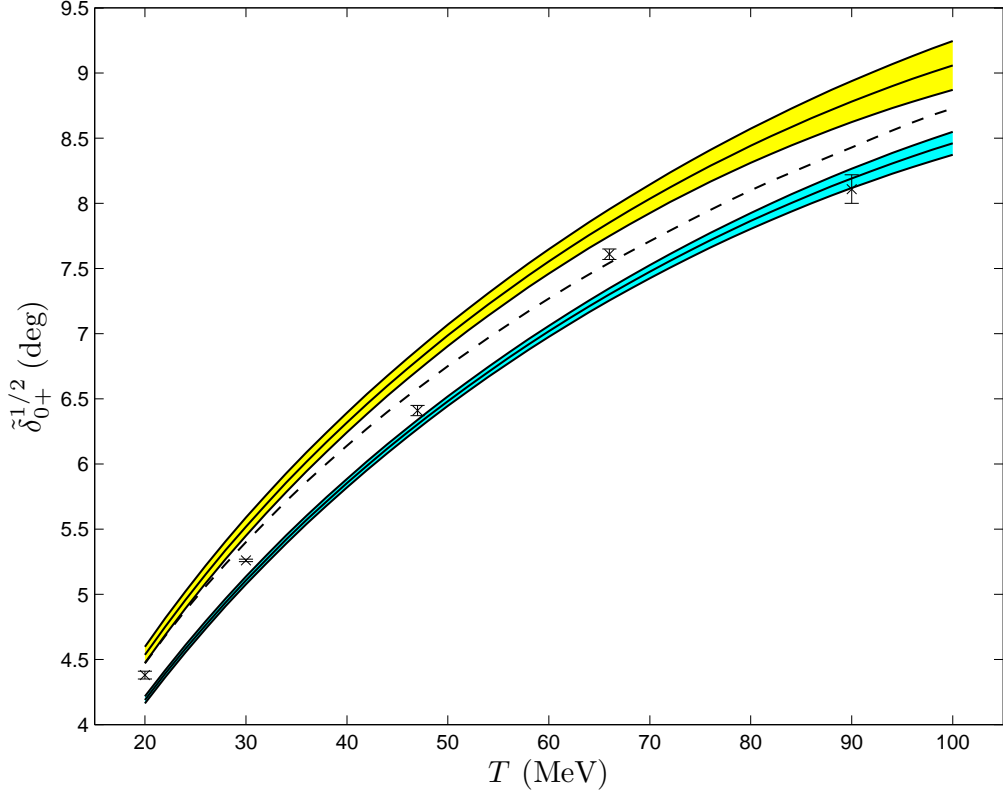


Fig. 2. The energy dependence of the em-modified hadronic phase shift $\tilde{\delta}_{0+}^{1/2}$ (S11) from the present work, along with 1σ uncertainties (yellow band). Also included is the ZUAS12 prediction [1], obtained on the basis of the elastic-scattering data below 100 MeV, along with the corresponding 1σ uncertainties (blue band). The current SAID solution (WI08) [23] is represented by the dashed curve; the five points shown (at $T = 20, 30, 47, 66, 90$ MeV) are the single-energy WI08 values.

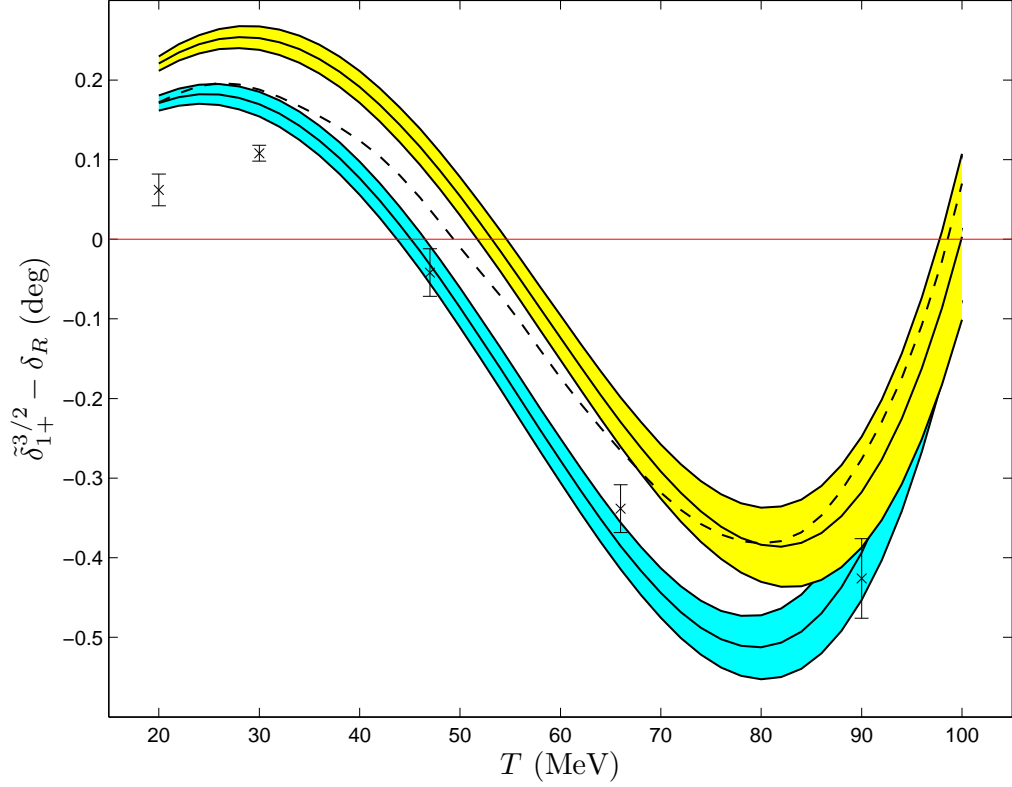


Fig. 3. The energy dependence of the em-modified hadronic phase shift $\tilde{\delta}_{1+}^{3/2}$ (P33) from the present work, along with 1σ uncertainties (yellow band). Also included is the ZUAS12 prediction [1], obtained on the basis of the elastic-scattering data below 100 MeV, along with the corresponding 1σ uncertainties (blue band). The current SAID solution (WI08) [23] is represented by the dashed curve; the five points shown (at $T = 20, 30, 47, 66,$ and 90 MeV) are the single-energy WI08 values. To enable a better comparison of the values contained in this figure, an energy-dependent baseline $\delta_R (= (0.20 \cdot T + 1.54)T \cdot 10^{-2}$, with T in MeV and δ_R in degrees) has been subtracted from all data.

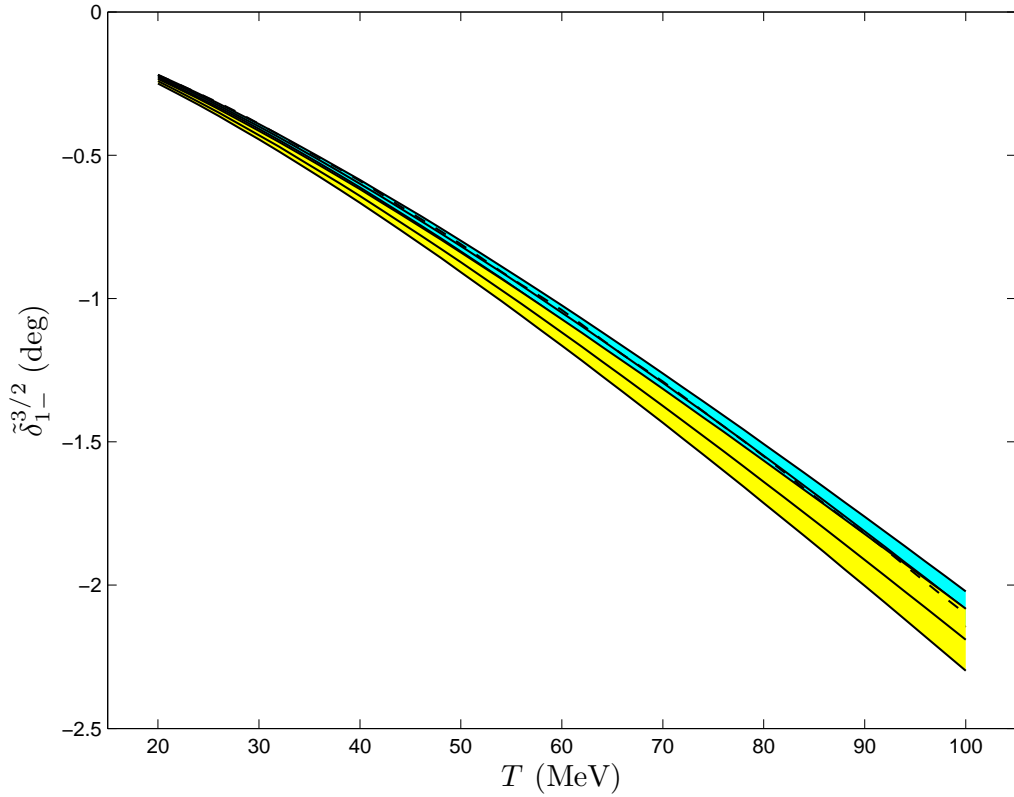


Fig. 4. The energy dependence of the em-modified hadronic phase shift $\tilde{\delta}_{1-}^{3/2}$ (P31) from the present work, along with 1σ uncertainties (yellow band). Also included is the ZUAS12 prediction [1], obtained on the basis of the elastic-scattering data below 100 MeV, along with the corresponding 1σ uncertainties (blue band). The current SAID solution (WI08) [23] is represented by the dashed curve.

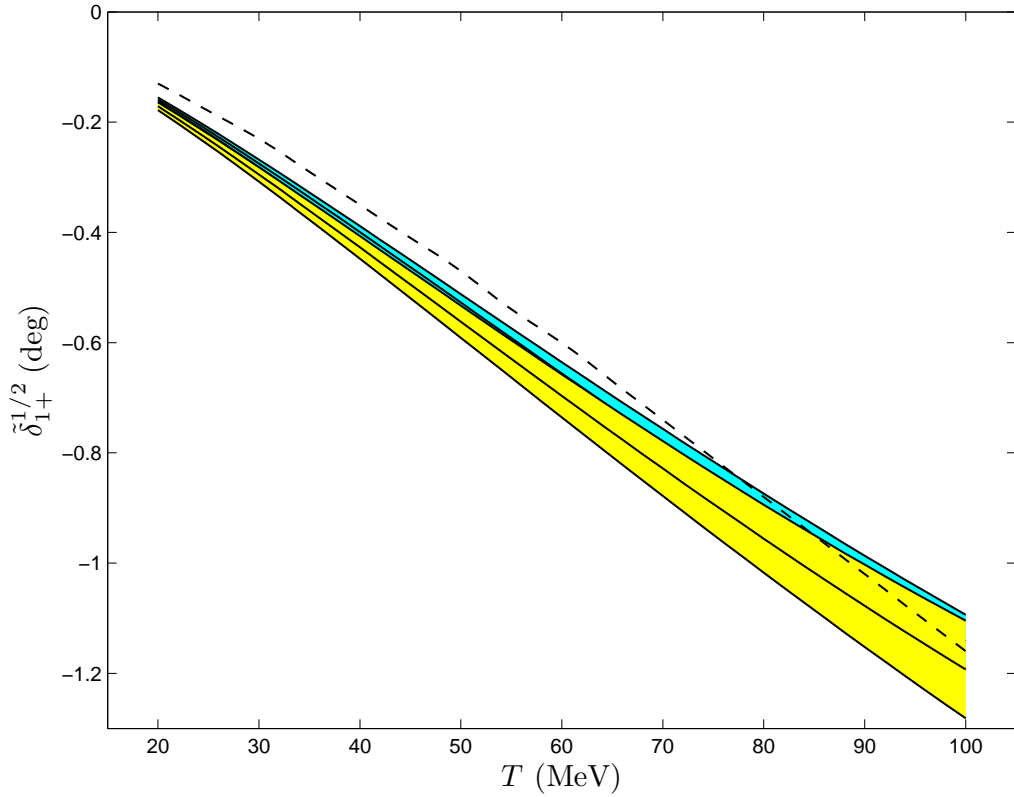


Fig. 5. The energy dependence of the em-modified hadronic phase shift $\tilde{\delta}_{1+}^{1/2}$ (P13) from the present work, along with 1σ uncertainties (yellow band). Also included is the ZUAS12 prediction [1], obtained on the basis of the elastic-scattering data below 100 MeV, along with the corresponding 1σ uncertainties (blue band). The current SAID solution (WI08) [23] is represented by the dashed curve.

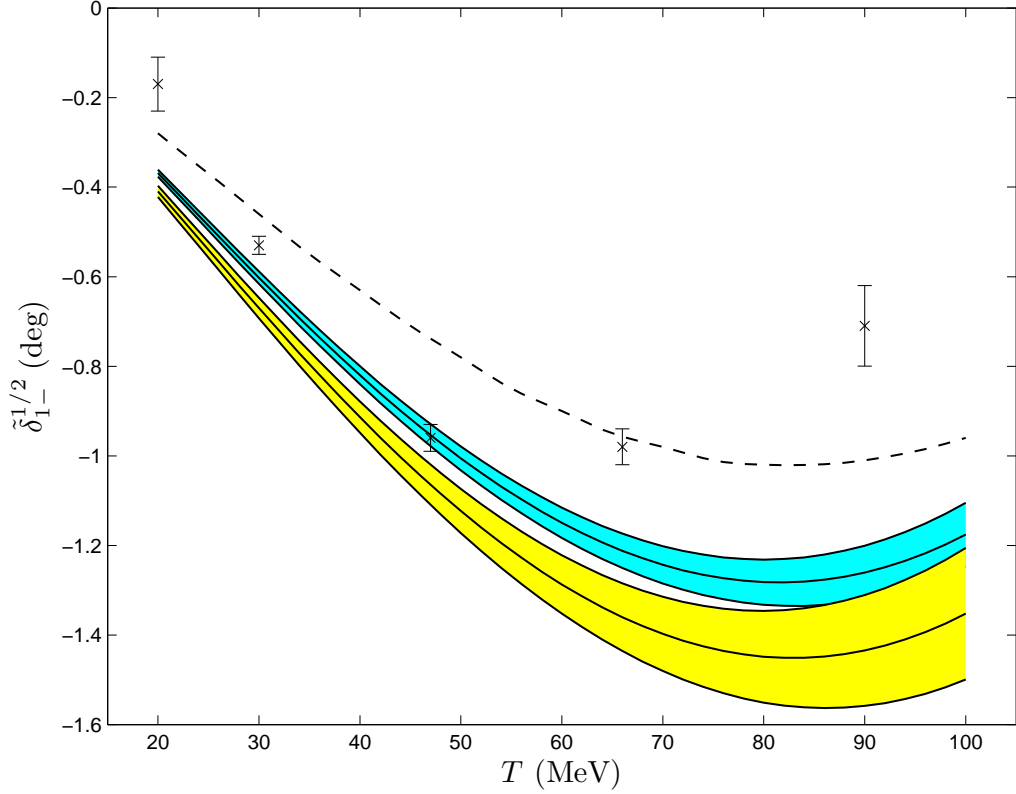


Fig. 6. The energy dependence of the em-modified hadronic phase shift $\tilde{\delta}_{1-}^{1/2}$ (P11) from the present work, along with 1σ uncertainties (yellow band). Also included is the ZUAS12 prediction [1], obtained on the basis of the elastic-scattering data below 100 MeV, along with the corresponding 1σ uncertainties (blue band). The current SAID solution (WI08) [23] is represented by the dashed curve; the five points shown (at $T = 20, 30, 47, 66, 90$ MeV) are the single-energy WI08 values.

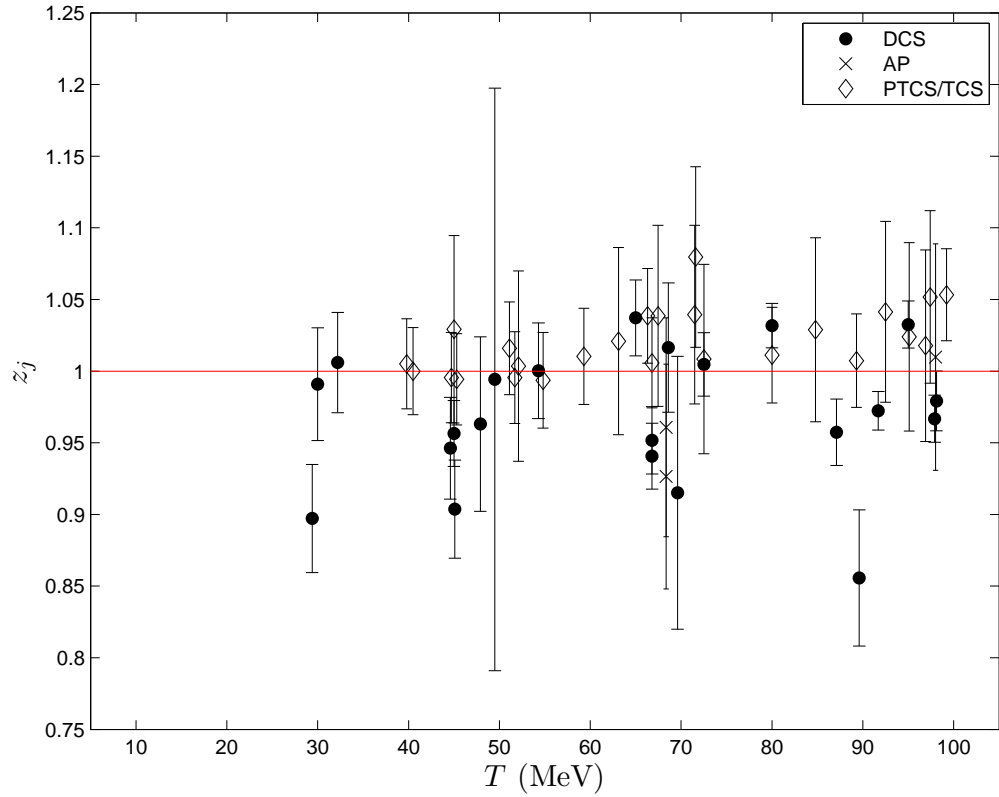


Fig. 7. The scale factors z_j of the π^+p data sets, obtained from the common fit to the truncated π^+p and CX databases using the ETH model (see Section 5.2). The values, corresponding to the two data sets which were freely floated (see Table 1 of Ref. [1]), have not been included. The results of the linear fit to the shown values are given in Section 5.2.3.

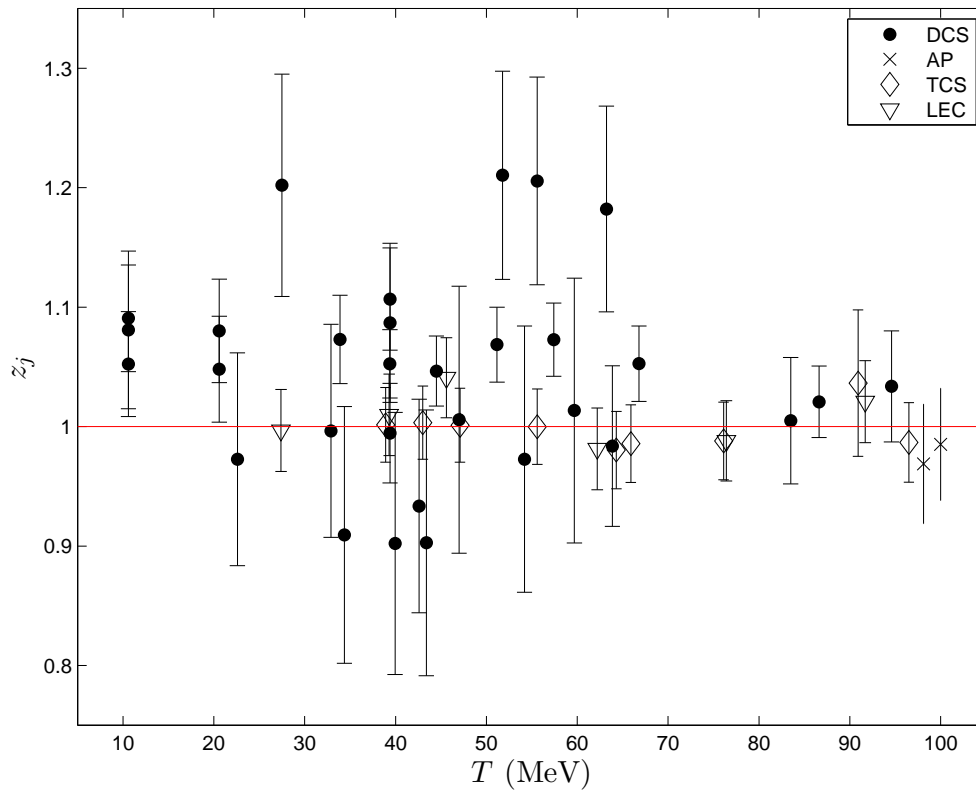


Fig. 8. The scale factors z_j of the CX data sets, obtained from the common fit to the truncated π^+p and CX databases using the ETH model (see Section 5.2). The values, corresponding to the four data sets which were freely floated (see Table 3), have not been included. The results of linear fits to the shown values are given in Section 5.2.3. The data sets with the largest scale factors z_j are the three remaining FITZGERALD86 data sets, as well as the FRLEŽ98 data set.

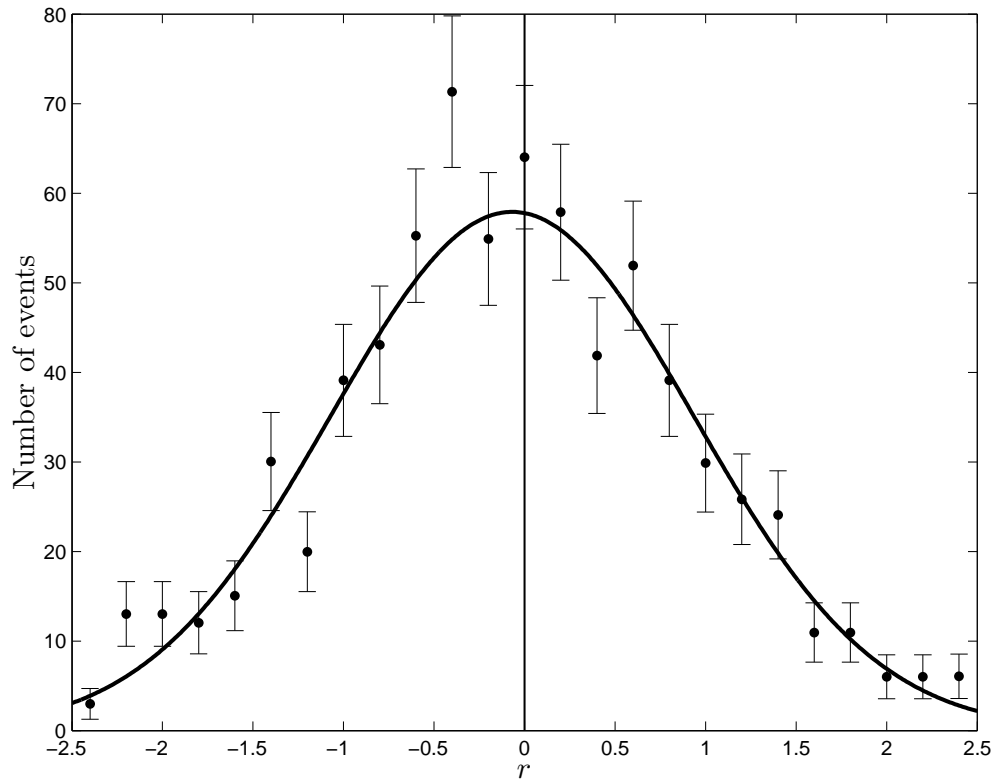


Fig. 9. The distribution of the normalised residuals, obtained from the common fit to the truncated π^+p and CX databases using the ETH model (see Section 5.2.3). Also shown is the optimal Gaussian fit to the data (solid curve).

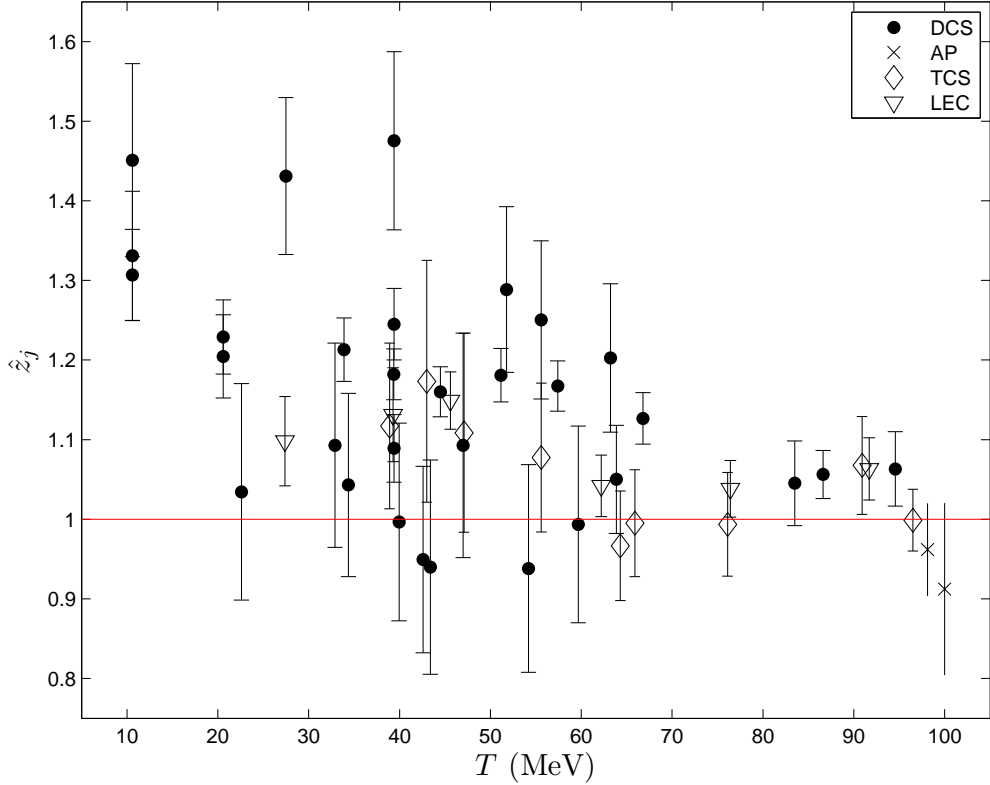


Fig. 10. The scale factors \hat{z}_j for free floating (evaluated with Eq.(5) of Ref. [1]) of the CX data sets, obtained on the basis of the ZUAS12 predictions [1], plotted separately for differential cross sections (DCS), total cross sections (TCS), analysing powers (AP), and the results for the coefficients of the Legendre expansion of the DCS (LEC). The four FITZGERALD86 data sets, which had been freely floated (see Table 3), as well as the BREITSCHOPF06 75.10 MeV entry, have not been included. Not shown in the figure is also the result of Ref. [17] for the isovector scattering length b_1 .

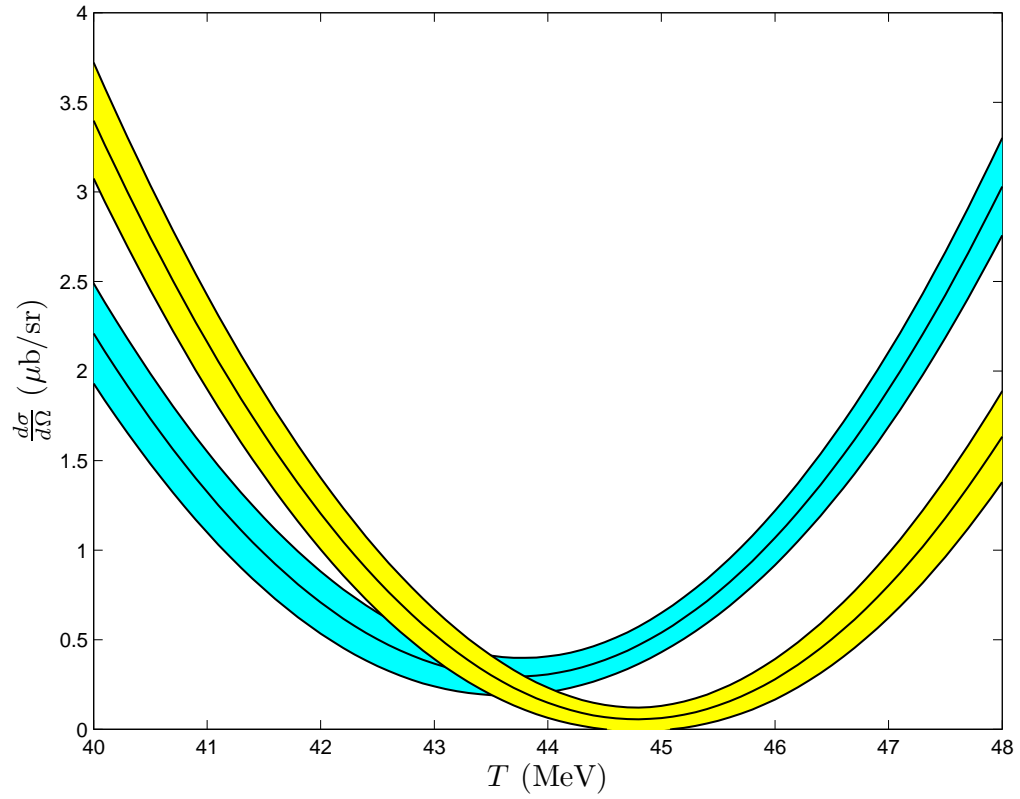


Fig. 11. Two predictions for the CX DCS for CM scattering angle $\theta = 0^\circ$ around the s - and p -wave interference minimum. The ZUAS12 prediction [1] is represented by the blue band, whereas the ZUAS12a one (this work) by the yellow band. Both bands indicate 1σ uncertainties.

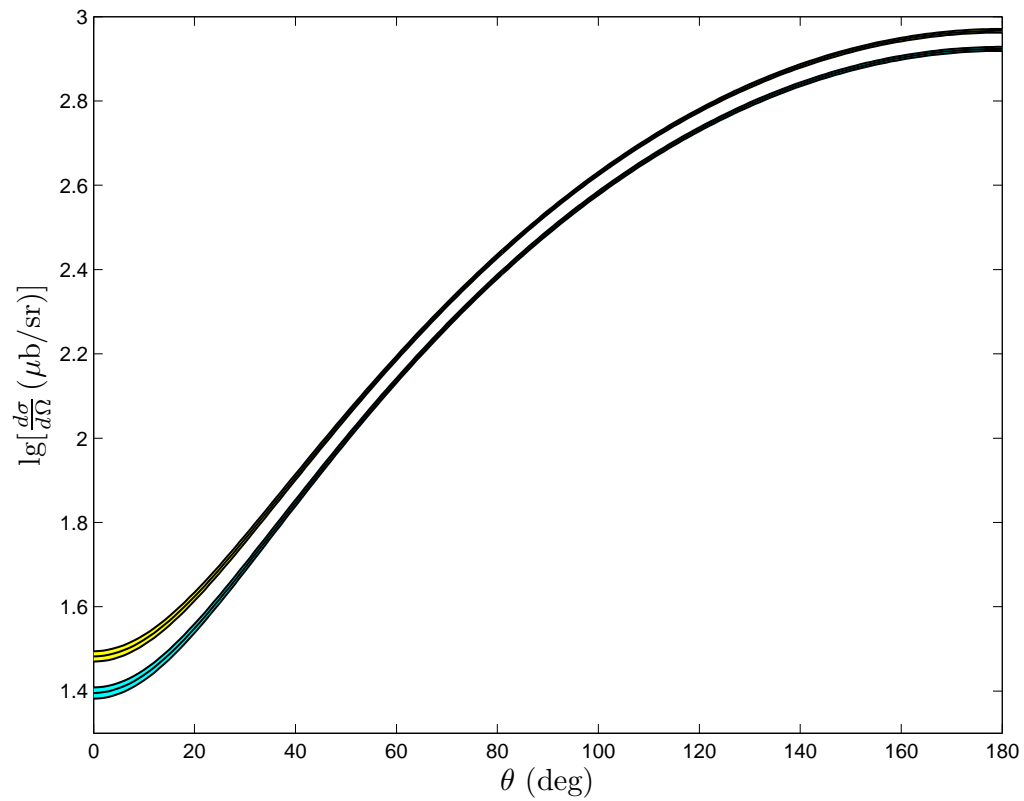


Fig. 12. Two predictions for the angular distribution of the CX DCS at 30 MeV; θ denotes the CM scattering angle. The ZUAS12 prediction [1] is represented by the blue band, whereas the ZUAS12a one (this work) by the yellow band. Both bands indicate 1σ uncertainties.

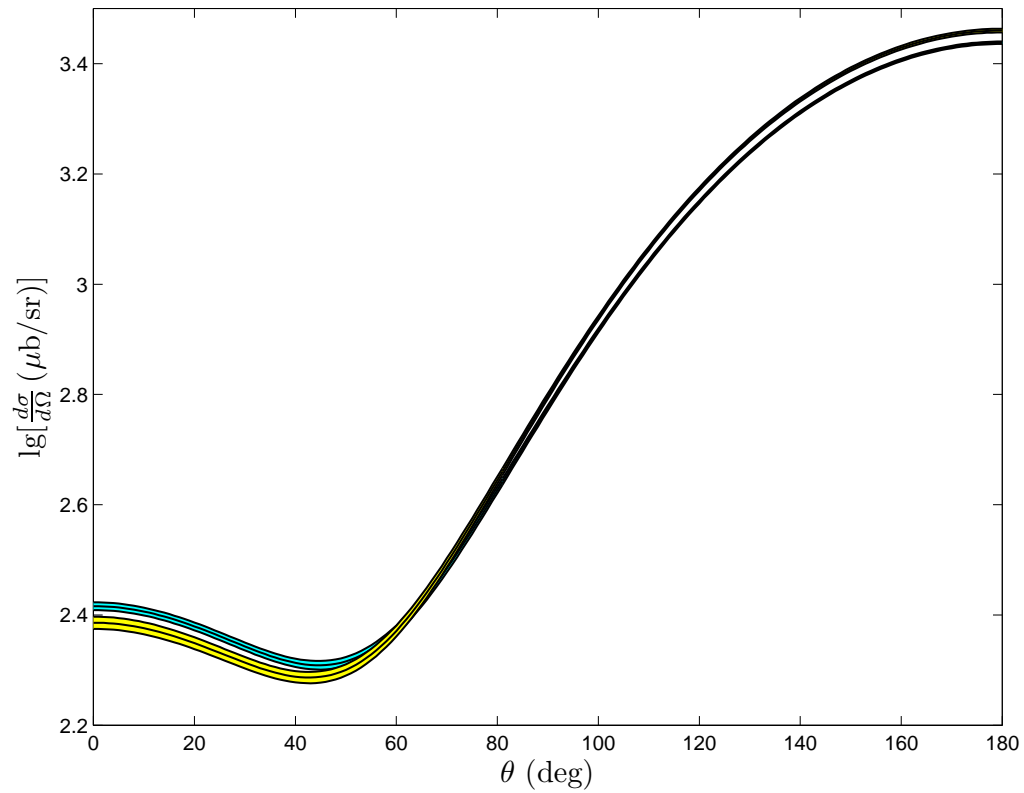


Fig. 13. Two predictions for the angular distribution of the CX DCS at 80 MeV; θ denotes the CM scattering angle. The ZUAS12 prediction [1] is represented by the blue band, whereas the ZUAS12a one (this work) by the yellow band. Both bands indicate 1σ uncertainties.

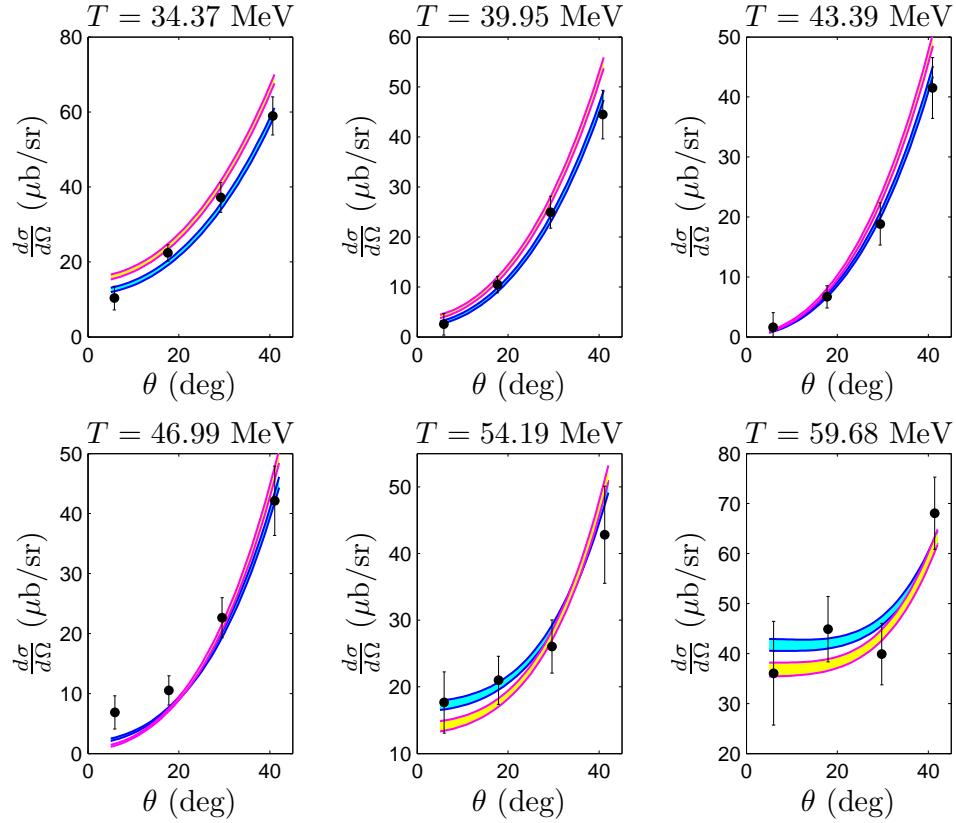


Fig. 14. Two predictions for the angular distribution of the CX DCS in the kinematical region of the JIA08 [20] experiment. The ZUAS12 prediction [1] is represented by the blue band, whereas the ZUAS12a one (this work) by the yellow band. Both bands indicate 1σ uncertainties. Only the statistical uncertainties of the measurements of Ref. [20] are shown (i.e., the 10% normalisation uncertainty of the experiment has not been included).

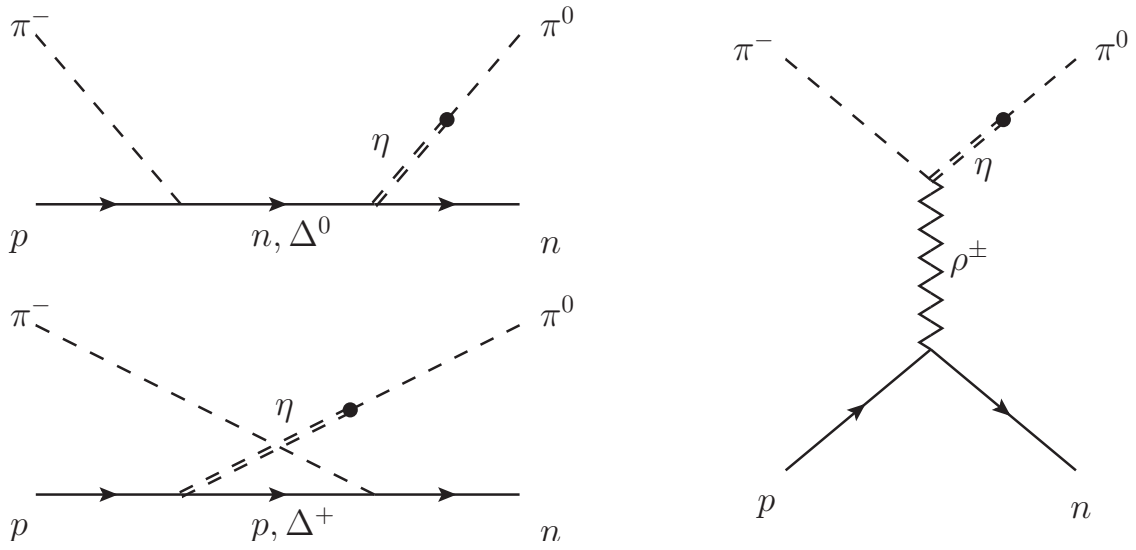


Fig. 15. Feynman graphs involving the $\eta - \pi^0$ mixing, a potential mechanism for the violation of the isospin invariance in the hadronic part of the πN interaction in the case of the CX reaction.